ACCEPTED BY AJ 2004 FEBRUARY 23
Preprint typeset using LaTeX style emulateapj v. 2/19/04

M/L, Hα ROTATION CURVES, AND H I GAS MEASUREMENTS FOR 329 NEARBY CLUSTER AND FIELD SPIRALS: II. EVIDENCE FOR GALAXY INFALL

NICOLE P. VOGT[1,2]
Department of Astronomy, New Mexico State University, Las Cruces, NM 88003
AND
MARTHA P. HAYNES,[3] RICCARDO GIOVANELLI,[3] AND TERRY HERTER
Center for Radiophysics and Space Research, Cornell University, Ithaca, NY 14853
Accepted by AJ 2004 February 23

ABSTRACT

We have conducted a study of optical and H I properties of spiral galaxies (size, luminosity, Hα flux distribution, circular velocity, H I gas mass) to explore the role of gas stripping as a driver of morphological evolution in clusters. We find a strong correlation between the spiral and S0 fractions within clusters, and the spiral fraction scales tightly with cluster X-ray gas luminosity. We explore young star formation and identify spirals that are (1) *asymmetric*, with truncated Hα emission and H I gas reservoirs on the leading edge of the disk, on a first pass through the dense intracluster medium in the cores of rich clusters; (2) strongly H I deficient and *stripped*, with star formation confined to the inner 5 h^{-1} kpc and 3 disk scale lengths; (3) reddened, extremely H I deficient and *quenched*, where star formation has been halted across the entire disk. We propose that these spirals are in successive stages of morphological transformation, between infalling field spirals and cluster S0s, and that the process which acts to remove the H I gas reservoir suppresses new star formation on a similarly fast timescale. These data suggest that gas stripping plays a significant role in morphological transformation and rapid truncation of star formation across the disk.

Subject headings: galaxies: clusters — galaxies: evolution — galaxies: kinematics and dynamics

1. INTRODUCTION

Some of the fundamental questions of galaxy formation are the following: Can we reconcile the observed galaxy populations at high redshifts with those found today in the local universe? Are the proposed mechanisms of interaction between galaxies and other galaxies or clusters sufficient to explain observations of galaxies within clusters and groups? Can we similarly explain the evolutionary history of field galaxies without invoking separate formation scenarios?

Studies of distant galaxies have established that there is significant evolution in cluster galaxy populations from redshifts z = 0.5 to the present. Butcher & Oemler (1978) first noted the excess of blue galaxies in the cores of rich clusters at redshifts as low as $z \sim 0.2$; many studies have since verified and extended this so–called "Butcher–Oemler effect". Parallel studies established that the fraction of spiral and S0s varied inversely within rich clusters, with the S0 fraction dropping by factors of 2-3 from local levels by redshifts $z \sim 0.5$ (Couch *et al.* 1994; Dressler *et al.* 1997; van Dokkum *et al.* 1998; Fasano *et al.* 2000). In contrast, the relatively constant numbers and tightly constrained colors of the cluster elliptical population indicated that it was very stable, with star formation concentrated at redshifts $z \geq 3$ (Ellis *et al.* 1997, though van Dokkum *et al.* 1999, 2000 suggest that progenitor bias may elevate the apparent formation redshift). Finally, optical spectra identified numerous poststarburst galaxies within clusters (Dressler & Gunn 1983, Couch & Sharples 1987), a suppressed star formation rate for spiral types relative to the field (Balogh *et al.* 1998), and found evidence of an infalling spiral population out to redshifts $z \sim 0.4$ (Poggianti *et al.* 1999; Kodama & Bower 2001).

In summary, these intermediate redshift studies support a well-known class of scenarios (*e.g.*, Spitzer & Baade 1951; Melnick & Sargent 1977 for early discussion) wherein rich clusters are continuously rejuvenated by infalling field spirals (Balogh, Navarro, & Morris, 2000); star formation is disrupted and morphology is slowly transformed, some turning into the S0 population of today (Jones, Smail, & Couch 2000; Kodama & Smail 2001; though see Andreon 1998).

The observational evidence obtained from studying local clusters and groups is more ambiguous. Dressler (1980a) argued strongly against the formation of S0s through transformation of spirals, citing their presence in low density, cool regions, the uniformity of the density-morphology relation in both relaxed and unrelaxed clusters, and the enhanced luminosity of S0 bulges relative to that of the complete spiral population. Solanes & Salvador-Solé (1992, and references therein) addressed the first two points by proposing that an initial correlation between density and bulge mass occurred during protogalaxy formation, leading to early bulges in pockets of initial overdensities. This innate bias could explain the continued morphology-density relation in low density regions, but would be erased from high density regions during vigorous stages of cluster formation. Accreted, gas stripped spirals could gradually build up the core S0 population afterward, thus restoring the morphology-density relation. Pfenniger (1993) addressed the third point with simulations that suggested that S0 bulges could be supplemented after disk formation by a burst of star formation, fueled by gas funneled to the nucleus via a short-lived bar. This mechanism would also explain the high metallicity gradients observed in the inner

Electronic address: nicole@nmsu.edu
Electronic address: haynes, riccardo, and herter@astro.cornell.edu

[1] Formerly at: Institute of Astronomy, University of Cambridge, Cambridge, CB3–0HA, UK

[2] Formerly at: Center for Radiophysics and Space Research, Cornell University, Ithaca, NY 14853

[3] National Astronomy and Ionosphere Center; NAIC is operated by Cornell University under a cooperative agreement with the National Science Foundation.

regions of bulges (Fisher, Franx, & Illingworth 1996).

The combination of low and intermediate redshift observations indicates that morphological transformation is significant within clusters, but there is much to be determined regarding the details of how it occurs. Three broad types of physical mechanisms have been proposed to model the transformation of spiral galaxies in dense environments: galaxy-galaxy interactions, tidal forces, and gas stripping. Galaxy-galaxy interactions are most efficient within groups, where relative velocities are low (Zabludoff & Mulchaey 1998; Mulchaey & Zabludoff 1998; Ghigna *et al.* 1998), and tidal forces (Toomre & Toomre 1972; Moore *et al.* 1996; Mihos, McGaugh, & de Blok 1997) are most effective on small spirals (though see Gnedin 2003a, 2003b). In spite of these factors, recent large-scale surveys (Lewis *et al.* 2002, Nichol *et al.* 2002) have found clear evidence of the significance of such moderate physical processes in suppressing star formation, particularly in galaxies located beyond cluster cores, though often at a extreme cost in morphological transformation (*e.g.*, harassment conversion into dwarf spheroidals).

Gas stripping mechanisms, in contrast, are extremely efficient at gas removal, while preserving the large-scale structure of spiral galaxy disks. They allow for a gradual fading of stellar populations, as H II regions diminish in intensity and surface brightness simultaneously decreases *and* becomes more uniform across the disk. Stripping can take on several forms, including absorption of a hot gas outer envelope (Larson, Tinsley, & Caldwell 1980), ram pressure sweeping (Gunn & Gott 1972), evaporation via turbulent mixing and heat conduction (Cowie & Songaila 1977), and turbulent viscous stripping (Nulson 1982). Hardware limitations (Steinmetz & Müller 1993; Steinmetz 1996) have precluded incorporating the effects into N-body simulations with gas dynamics at adequate resolution and coverage (time steps and size scales), though recent models of ram pressure stripping of individual Virgo spirals have been quite successful (Abadi, Moore & Bower 1999; Vollmer *et al.* 1999, 2000, 2001a, 2001b; Vollmer 2003; Vollmer & Huchtmeier 2003).

Observational studies of the H I gas dynamics (*cf.* Giovanelli & Haynes 1985; Magri *et al.* 1988; Solanes *et al.* 2001) have found a strong correlation between H I deficiency and clustercentric radius throughout a range of local clusters, strongest in early type spirals (Dressler 1986, though note Koopmann & Kenney 1998), and that while H I deficiency can extend as far out as 3 h^{-1} Mpc most gas stripping occurs well within cluster cores, within galaxies on preferentially radial orbits (Solanes *et al.* 2001). Cayatte *et al.* (1990, 1994) obtained aperture synthesis H I maps of Virgo cluster galaxies and found signatures of ram pressure and of viscous stripping in separate populations, distinguished by the ratio of H I to optical diameters, while Bravo-Alfaro *et al.* (1997, 2000, 2001) have used a similar technique to identify first pass spirals falling into and out of the core of Coma and around A262.

An alternate technique is to examine the properties of Hα rotation curves of local cluster spirals. Early pioneering studies (Rubin, Whitmore, & Ford 1988; Whitmore, Forbes, & Rubin 1988; Forbes & Whitmore 1989) suggested that velocity profiles declined at large optical radii more in cluster spirals than in the field, implying gas stripping or diminished halos, but this result has not been supported by later observations (Distefano *et al.* 1990; Amram *et al.* 1993; Sperandio *et al.* 1995; Vogt 1995). A recent, large-scale study of 510 rotation curves (Dale *et al.* 2001) found instead weak trends in the extent and asymmetry of the Hα flux with clustercentric radius, but the strong selection bias towards late type spirals (Dale *et al.* 1999) with strong, extended Hα or [N II] 6584Å emission constrains the application of this result to the general cluster spiral population.

In this paper, we identify and explore a population of infalling spirals in a large sample of spiral galaxies, 296 selected from 18 nearby clusters and 33 isolated field galaxies observed for comparative purposes. The current program integrates both optical and H I observations and is thus sensitive to both gas depletion and star formation suppression. The targeted galaxies are spread over a wide range of environments, covering three orders of magnitude in cluster X-ray luminosity and containing galaxies located throughout the clusters from rich cores out to sparsely populated outer envelopes. We have obtained Hα rotation curves to trace the stellar disk kinematics within the potential at high resolution and to explore the strength of current star formation, H I line profiles to map the overall distribution and strength of H I gas, and *I*-band imaging to study the distribution of light in the underlying, older stellar population. The sample contains spirals of all types, and is unbiased by the strength of flux from H II regions or by H I gas detection. This paper is a companion to Vogt, Haynes, Herter & Giovanelli (2004a, Paper I), which details the observations and reduction of the data set, and to Vogt, Haynes, Giovanelli & Herter (2004b, Paper III), which explores changes in the fundamental parameters (size, luminosity, and mass) and star formation properties of spiral galaxies as a function of the cluster environment.

2. DESCRIPTION OF CLUSTERS

2.1. *Characterization*

As discussed in Paper I, we have selected a set of local clusters and groups which span a wide range of environments, parameterized by X-ray luminosity and velocity dispersion, richness, substructure, and spiral fraction. Table 1 lists the complete set, hereafter referred to as the cluster sample, ordered by X-ray temperature, and compares them under several forms of cluster classification. We include two estimates of the morphological fraction, one taken from the literature, and a second determined from all galaxies with measured positions and redshifts within 2 h^{-1} Mpc of the cluster center. The latter measure incorporates all cataloged galaxies, referred to as the "parent sample", encompassing the same volume and to the same depth, as our spiral galaxy study. Galaxies with measured redshifts within 6° (5 to 10 h^{-1} Mpc) of each cluster center were selected; the assembled galaxies range from 10 to 22 in *B*-band magnitudes, peaking at 15.5 magnitudes. As discussed below, a subsample comprised of $\sim$ 300 spiral galaxies inclined more than 30° from face-on orientation was then drawn from the parent sample, to serve as targets for a detailed dynamical study of the process of spiral infall.

The initial cluster galaxy sample was drawn from the 1994 version of the private database of R.G. and M.P.H. known as the AGC , including objects contained within the UGC and CGCG galaxies, objects included in the cluster sample of Dressler (1980b) and objects identified by eye examination of the POSS prints.

We supplemented these data with those for additional galaxies archived within the NASA/IPAC Extragalactic Database[4] (NED), and the results of numerous local redshift surveys.

[4] The NASA/IPAC Extragalactic Database is operated by the Jet Propulsion Laboratory, California Institute of Technology, under contract with the National Aeronautics and Space Administration

TABLE 1
CLUSTER PROPERTIES

Cluster	kT[a]	log L_x[b]	σ[c]	V_{pec}[d]	Cluster Classification[e]				Membership[f]		Ref.
	(keV)	(erg s^{-1})	(km s^{-1})		J-F	R	B-M	R-S	(E:S0:Sp)		
(1)	(2)	(3)	(4)	(5)	(6)	(7)	(8)	(9)	(10)	(11)	(12)
A1656	8.3	45.10	997	170	evolved nXD	2	II	B	28:50:22	35:47:18	1,4,13
A426	6.2	45.36	1307	-364	evolved XD	2	II–III	L	30:30:41	48:45:07	1,5,14
A2199	4.7	44.81	823	-235	int. XD	2	I	cD_p	23:31:46	35:41:24	1,6,13
A2147	4.4	44.58	821	303	early XD	1	III	F	11:24:66	27:31:42	1,6,15
A2063	4.1	44.47	626	680	int. XD	1	II–III	cD_p	13:41:46	38:13:49	1,6,16
A2151	3.8	44.00	705	312	early XD	2	III	F	13:19:68	14:35:51	1,7,13
A1367	3.7	44.23	802	43	early nXD	2	II–III	F	11:26:63	17:40:43	1,6,13
A2634	3.4	44.12	661	-82	early nXD	1	I–II	cD	17:42:41	17:47:36	1,8,16
A539	3.0	43.80	701	-277	nXD	1	III	F	07:42:51	19:53:28	1,9,13
A262	2.4	43.93	575	-32	early XD	0	III	I	09:32:59	17:36:47	1,10,14
A400	2.1	43.82	621	-250	int. XD	1	II–III	I	09:34:58	15:56:29	1,6,13
A2152	2.1	43.49	715	···	nXD	1	III	I	12:28:60	38:29:33	2,6,15
A2666	(1.7)	(42.00)	476	-156	···	0	I	cD_p	15:32:52	20:37:43	2,11,14
A2197	1.6	43.08	550	-282	nXD	1	II	L	15:03:82	19:36:45	2,6,13
N507	(1.6)	···	444	242	nXD	0	III	F	11:30:59	: :	2,10
A779	1.5	42.95	503	-100	···	0	II	cD_p	03:10:86	04:12:85	2,6
A2162	(0.9)	42.95	323	···	nXD	0	II–III	I	11:05:84	11:06:83	2,6
Cancer	(0.9)	< 42.30	317	250	nXD	0	III	I	18:12:70	11:18:71	3,12

[a]X-ray temperatures from Wu, Fang, & Xu (1998), and [b]bolometric luminosity; parenthesized values derived from velocity dispersion.

[b]Central velocity dispersion

[c]Peculiar velocity, taken from Giovanelli *et al.* (1997); derived in consistent fashion for additional clusters.

[d]Rankings under Jones-Forman, Abell richness, Bautz-Morgan, and Rood-Sastry classification systems.

[e]Morphological ratio for members out to 2 h^{-1} Mpc, and from the literature (drawn from inner 1.5 h^{-1} Mpc).

X-ray data taken from (1) David *et al.* (1993), (2) Abramopoulos & Ku (1983, (3) Giovanelli & Haynes (1985). Velocity dispersions taken from (4) Kent & Gunn (1982), (5) Kent & Sargent (1983), (6) Zabludoff *et al.* 1993, (7) Bird, Dickey, & Salpeter (1993), (8) Scodeggio *et al.* (1994), (9) Ostriker *et al.* (1988), (10) Sakai, Giovanelli, & Wegner (1994), (11) Struble & Ftaclas (1994), (12) Bothun *et al.* (1983). Morphological ratios taken from (13) Oemler (1974), (14) Melnick & Sargent (1977), (15) Tarenghi *et al.* (1980), (16) Dressler (1980b).

The combined number of galaxies with measured redshifts within 4σ and 2 h^{-1} Mpc for each cluster ranges from 35 for the poorest cluster A2162 to 583 for the rich A1656, with a median value of 121. This parent sample starts to become significantly incomplete at *B*-band magnitudes ranging from -18.5 to -19.5 over the redshift range of the sample ($z = 0.016$ to 0.037). However, data from the well-studied cluster A1656 (Coma) extend more than a full magnitude deeper. The sample is comprised of clusters with well-studied dynamics, and thus while it is not strictly complete in magnitude, size, or volume, it is assumed to be fairly complete to roughly two magnitudes below L^* for cluster members within 3 h^{-1} Mpc of the cluster centers.

2.2. *Distribution of Parent Sample of Galaxies*

Figures 1 through 3 show the distribution of galaxies within the parent sample around each cluster, on the sky and in radial velocity space. The clusters have been sorted in order of decreasing X-ray temperature; for the purposes of discussion, we divide the sample between *hot* and *cold* clusters, at $kT_{gas} = 3$ eV. Figure 2 shows the distributions for hot clusters, while Figure 3 shows similar displays for the cold ones; the Coma cluster is illustrated individually in Figure 1. Galaxies are restricted to the range 4σ (velocity dispersion) about each cluster. This criterion is relaxed to 6σ for NGC 507 and Cancer to show the multiple subclumps within each group, as we have chosen to use the velocity dispersion of the dominant subgroup (listed in Table 1) rather than of the entire population. We selected spirals within 2 h^{-1} Mpc at the highest priority for our dynamical study, starting at the cluster centers and spiraling outwards. Despite this weighting scheme, we have observed no spirals within 200 h^{-1} kpc and 1σ of any of the cluster cores. This is not surprising, particularly for the hot clusters where many of the cluster centers are defined as the position of a cD galaxy. The cD halo alone could extend this far, and any spiral drawn this near would be subsumed by tidal forces.

Galaxies have been divided into ellipticals, S0s, and spirals to illuminate morphological segregation, as well as the enhanced overall density of galaxies in the cores. Targets of our dynamical study are further identified by larger concentric symbols according to their relationship to the cluster: true cluster members (circles), galaxies associated with the cluster potential and thus infalling (squares) and foreground and background galaxies (diamonds). The designation of true cluster member has been reserved for galaxies within the main

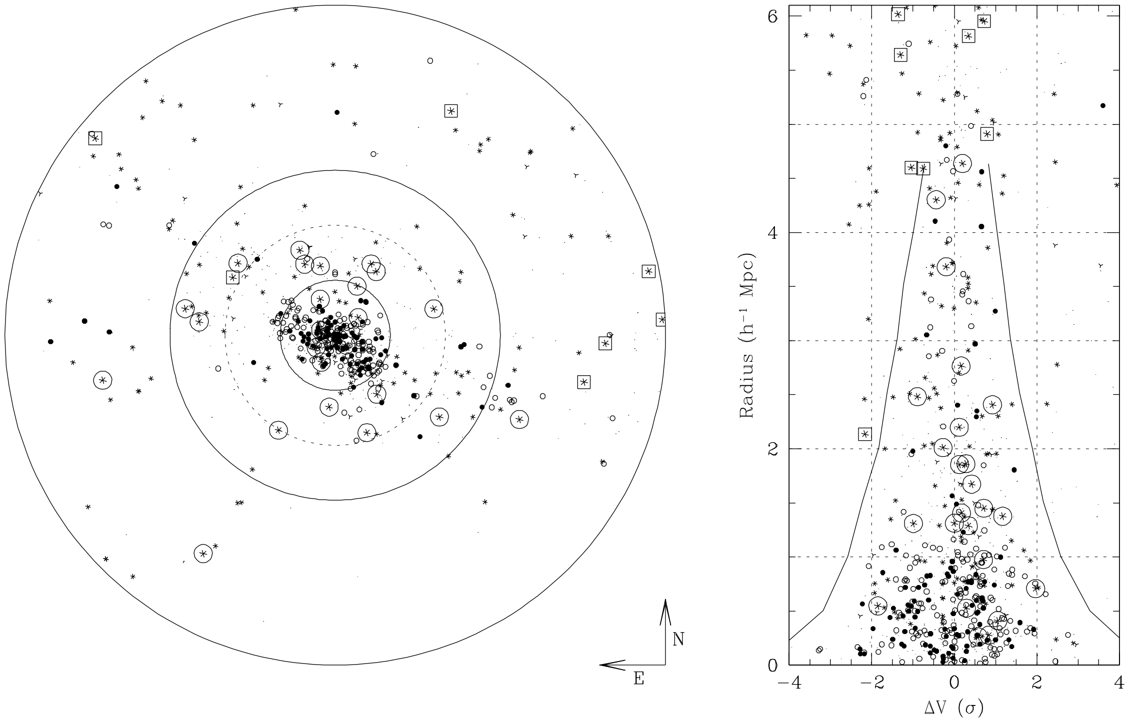

FIG. 1.— Distribution of galaxies within 6 h^{-1} Mpc and 4σ of hot cluster A1656 (Coma). Galaxies are drawn as ellipticals (filled circles), S0s (open circles), spirals (asterisks), irregulars (skeletal triangles) and untyped (small dots). Those within our dynamical sample are surrounded by circles (cluster members), squares (galaxies associated with the cluster), or diamonds (foreground and background galaxies, none within A1656). The rectangular plot shows the radial velocity distribution, in units of the cluster velocity dispersion; the membership caustic is taken from Kent & Gunn (1982). The round plot shows the spatial distribution of galaxies around the cluster, with circles drawn at 1, 2, 3, and 6 h^{-1} Mpc. It extends to show ten galaxies at radii well beyond 3 h^{-1} Mpc; we have sampled the extended supercluster structure more here than around the other clusters. Though beyond the cluster proper, these galaxies fall at the same redshift and are part of a larger unbound structure.

envelope of the cluster, while associated galaxies (either at rest with respect to the cluster at large radii, or, less commonly, in the inner few Mpc with a substantial velocity offset). The most significant complication in applying membership criteria lies at radii beyond 1 h^{-1} Mpc, in the removal of contamination from neighboring clusters, as discussed in Figures 2 and 3. The associated galaxies identified to be infalling into the cluster potential may also include true members on extreme radial orbits which have already passed through the center of the cluster. True cluster members are assumed to be at rest with respect to the cluster, while the associated members are taken to be at distances corresponding to their individual redshifts. The distinction is most relevant for galaxies offset in velocity from the cluster center.

Figure 4 (top) summarizes the morphological type distribution across the parent sample, where the clusters have been ordered by increasing spiral fraction, calculated from all cataloged galaxies with 2 h^{-1} Mpc. It should be noted that the spiral fractions derived from the literature typically refer to a smaller volume (< 1.5h^{-1} Mpc), whereas those derived from our parent galaxy incorporation include a greater contribution from the outer, typically spiral-richer regions. The general trend is that the spiral fraction varies inversely with the X-ray temperature of the cluster. It includes rich clusters A1367 and A2151 with high spiral fractions, while poor clusters A2666 and NGC 507 have few members but contain a high fraction of S0s. The high spiral fraction within A2147, in contrast, is expected, given that 90% of the X-ray luminosity is contributed by an AGN rather than by diffuse gas (Ebeling *et al.* 1996). The fraction of ellipticals within the clusters is relatively constant, hovering around 15% regardless of X-ray temperature or spiral fraction, and below 25% for all but two clusters, and there is a high correlation ($r = 0.94$) between counts of elliptical and S0 members; note that this has been observed out to redshifts beyond $z \sim 0.5$ (*cf.* Dressler *et al.* 1997). We find an equally strong inverse correlation ($r = -0.92$) between the *fraction* of spirals and of S0s which make up the remaining 85%. This trend holds across a range of cluster membership algorithms, and is evident in samples extending out to between 1 and 3 h^{-1} Mpc, beyond the virial radius of even the richest clusters where the density drops to $\lesssim 3$ (h^{-1} Mpc)^2 galaxies, and in the morphological ratios assembled from heterogeneous cluster surveys in the literature.

We find a moderately strong correlation ($r = -0.70$) between spiral fraction and X-ray gas luminosity or temperature (dropping to $r \sim 0.5$ for S0s or ellipticals), though no significant difference that might allow us to explore the relationship between intracluster gas density and the cluster potential (*i.e.* mass) within the clusters. Edge & Stewart (1991) have reported a much stronger correlation ($r = -0.96$ for luminosity, -0.85 for kT$_{gas}$) for a similarly sized sample, restricted to clusters with solid EXOSAT detections and kT$_{gas} > 2$ eV, but we do not reproduce it within the hotter portion of our sample. The stronger correlation, across the entire sample, is in fact between the X-ray gas luminosity and the temperature ($r = 0.92$).

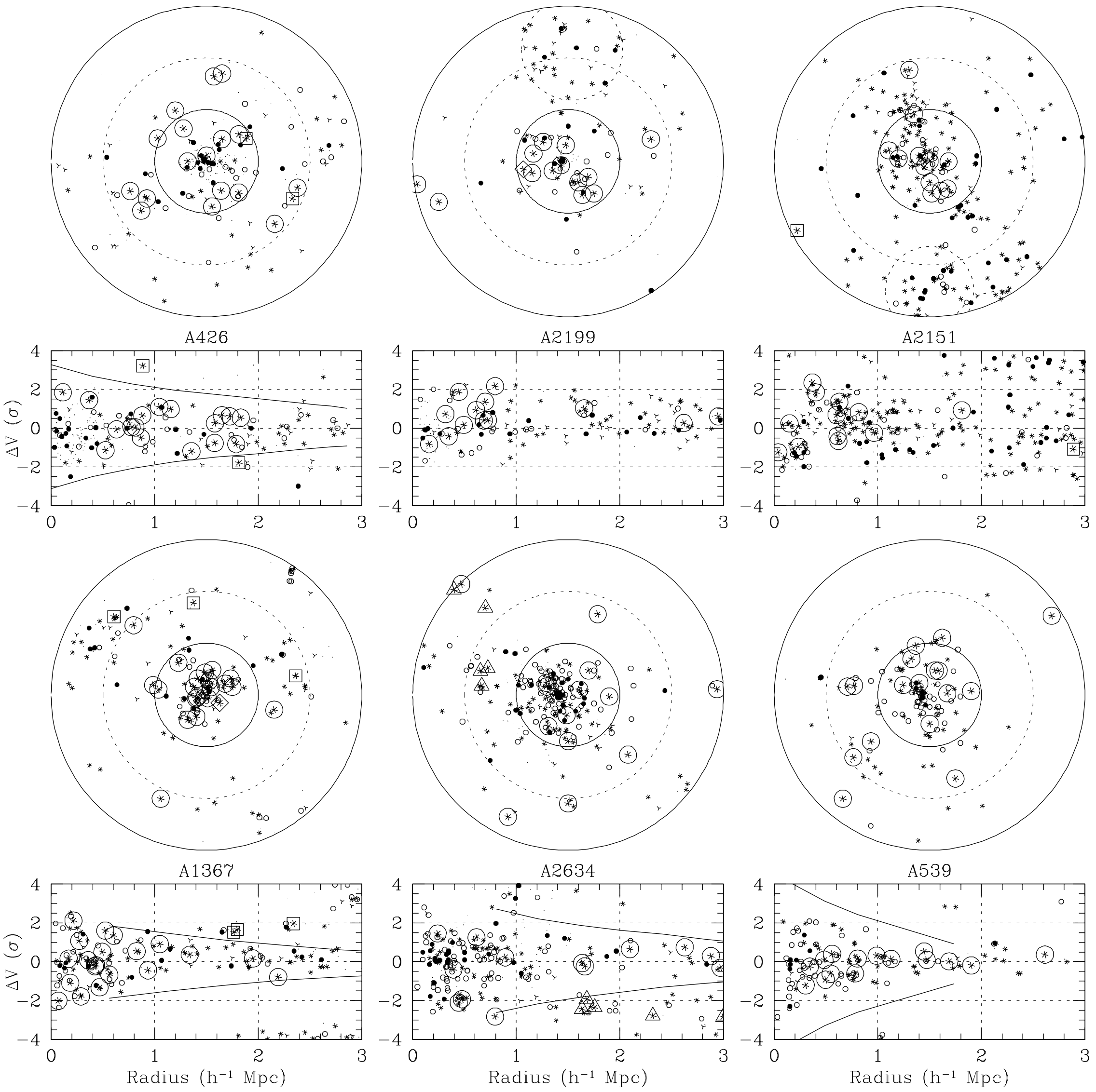

FIG. 2.— Distribution of galaxies within 3 h^{-1} Mpc and 4σ of hot clusters, with clusters ordered in decreasing X-ray temperature; symbols are as in Figure 1, and members of the infalling foreground group A2634-F around A2634 are surrounded with triangles. The round plots show the spatial distribution of galaxies, with circles drawn at 1, 2, and 3 h^{-1} Mpc and neighboring clusters marked with dashed circles at 1 h^{-1} Mpc. Membership caustics are shown for A426 (Kent & Sargent 1983), A1367 (Giovanelli *et al.* 1997a), A2634 (Scodeggio *et al.* 1995), and A539 (Ostriker *et al.* 1988). Galaxies were partitioned between A2197 and A2199 along a dividing line at 40° 30′. Hercules supercluster membership was originally established by breaking the sample into galaxies north of 17° (A2151), and then galaxies east (A2152) and west (A2147) of 16° 03′, and then updated in accordance with the extensive kinematic study of Barmby & Huchra (1998).

We define an overall measure, R, of the distance of each galaxy from its host cluster center by normalizing and combining the radial and velocity offsets. We equate a velocity offset of 3σ with a distance offset of 2 h^{-1} Mpc, such that, for radius r in units of h^{-1} Mpc and velocity v in units of σ,

$$R = \sqrt{r^2 + (\frac{2}{3}v)^2}\ h^{-1}\mathrm{Mpc}. \quad (1)$$

Figure 4 (bottom) shows the distribution of mean values of R for each morphological type within the clusters, where we have relaxed our membership criteria to include galaxies out to 3 h^{-1} Mpc within 3σ. The spiral population (both early and late types) has a relatively constant mean of 1.5 h^{-1} Mpc across the sample, representative of the spiral envelope which surrounds all of the cluster cores. Ellipticals match the spiral distribution in poor clusters, but in the rich clusters the mean falls to a more centrally concentrated 0.85 h^{-1} Mpc. This trend may be paralleled in the S0s, though the scatter is considerable. The velocity offset differences among morphological populations are negligible; this effect is driven by the radial distribution and the high concentration of ellipticals found in the cores of the rich clusters.

Figure 5 shows the distribution of mean R values for ellipticals, S0s, and spirals within each cluster, for members within $\frac{1}{2}$ h^{-1} Mpc and 5σ or within 2 h^{-1} Mpc and 3σ, with neighboring clusters removed. The plots extend to 3 h^{-1} Mpc in R, and the bulk of the cluster members fall within 2 h^{-1} Mpc. Galaxies within the sample which fall beyond these limits

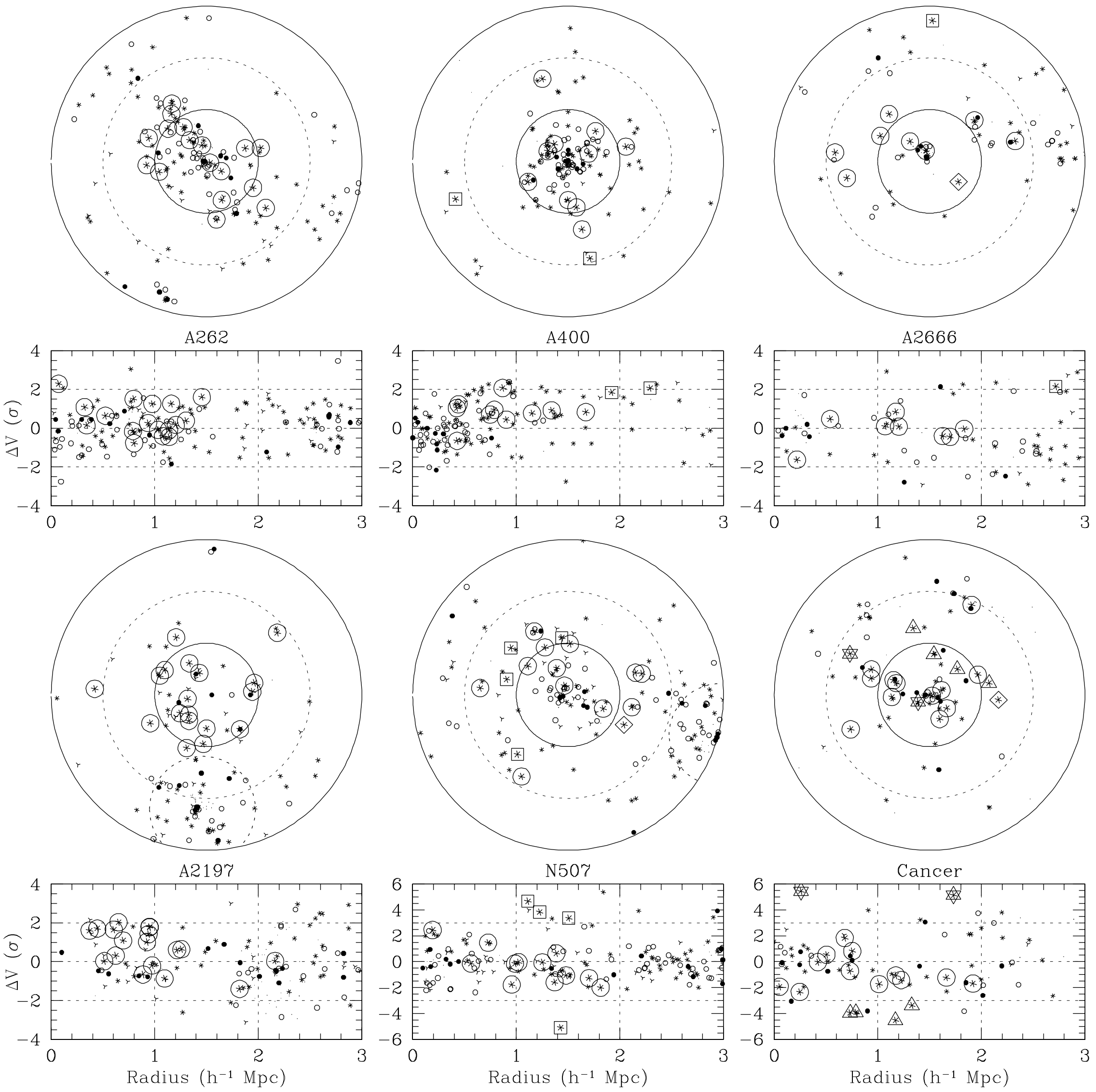

FIG. 3.— Distribution of galaxies within 3 h^{-1} Mpc of cold clusters, with clusters ordered in decreasing X-ray temperature; symbols as in Figure 1. The round plots show the spatial distribution of galaxies, with circles drawn at 1, 2, and 3 h^{-1} Mpc and neighboring clusters marked with dashed circles at 1 h^{-1} Mpc. The Cancer and NGC 507 cluster radial velocity diagrams are extended to 6σ to show infall and the main subclumps within Cancer (as defined in Bothum *et al.* 1983); galaxies within our sample are surrounded by circles (clump A members), stars (clump B or C members), triangles (clump D members), or diamonds (background galaxy).

(*e.g.*, spirals in the outer regions of the cluster environs, background and foreground galaxies) are thus not included on these plots, nor in the counts of galaxies of each type listed below the name of each cluster. The distribution was determined by applying a fixed-width kernel density estimate (Silverman 1986) to the raw R values, to achieve smoother representation than a standard histogram. An Epanechnikov kernel (inverted parabola) with a width of 0.5 R was used for the entire data set; selected by applying least-squares cross-validation to the distribution of each morphological type within each cluster.

The effects of morphological segregation can be clearly seen in the relative proportions of early to late type galaxies, ranging from the S0 dominated and elliptical rich A1656 down to poor clusters such as A779, composed almost entirely of spirals. As in Figure 4, we observe both rich clusters with high spiral fractions well within the potential and poor clusters with a significant number of S0s. These data will also be used to evaluate the validity of the subsampling of the parent spiral galaxy population in the selection of the spirals that comprise our dynamical sample.

2.3. *Distribution of Dynamical Subsample of Galaxies*

For a sample of 329 spiral galaxies, 296 in the vicinity of the clusters listed in Table 1, we have obtained Hα rotation curves to trace the stellar disk kinematics and the extent of young star formation, H I line profiles to map the overall distribution and strength of H I gas, and *I*-band imaging to study the distribution of light in the underlying, older stellar populations. We have one or more optical spectra for every targeted galaxy. However, it was not possible to survey all of the clusters within the sample to completion because of var-

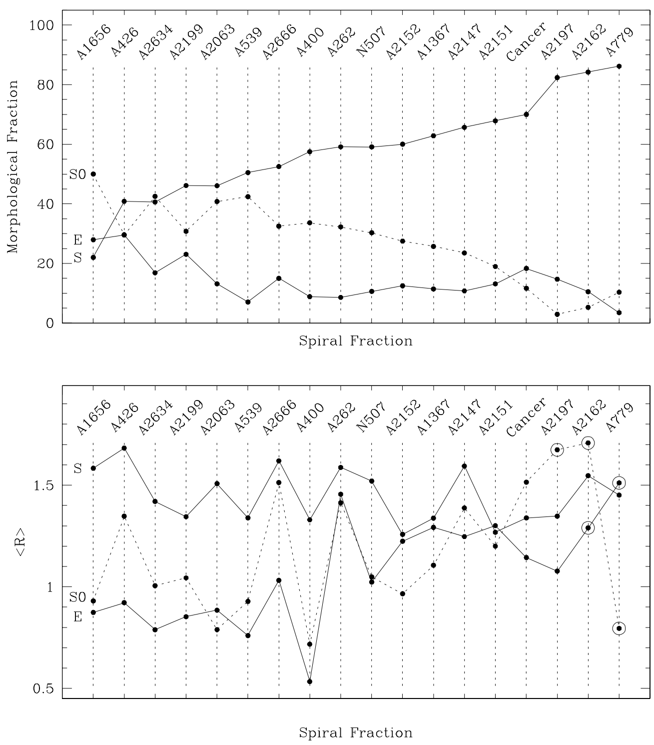

FIG. 4.— Distribution of relative morphological fractions **(top)** and mean values of the offset, R, **(bottom)** for ellipticals, S0s, and spirals within each cluster. Clusters are ordered by spiral fraction. Points are circled when the mean of the offset R was determined from fewer than five points. The fraction of ellipticals stays around 15%, while there is a clear inverse correlation (r = –0.92) between the fraction of spirals and S0s. The mean R value for spirals is relatively constant across the sample. Ellipticals are distributed similarly to spirals in the poor clusters, while those in the rich, hot clusters are far more centrally concentrated.

ious observational constraints (*e.g.*, adverse weather conditions, successful acquisition of a photometric optical image and H I line profile for each new galaxy with an optical spectrum). We must thus examine each cluster sample individually to determine whether the observed galaxies comprise a valid representation of the parent cluster spiral population.

In the evaluation of sample validity, we examine the final observational sample according to five criteria. Three refer to the size and extent of the targets: (1) We must have obtained 15 or more optical spectra in the region of each cluster, and this sample must not be biased against galaxies undetected in H I . This number includes true cluster members, galaxies associated with the cluster (*e.g.*, infalling spirals on the outskirts), and foreground and background galaxies; together these are designated as the *observed sample*. (2) We must have obtained 10 or more optical spectra of true cluster members within the observed sample. The distinction between true members, associated galaxies, and foreground and background galaxies has been made for each observed galaxy on a case by case basis by examining the parent distribution of galaxies on the sky and in radial velocity space (see Figures 1 through 3). (3) If H I line profiles and optical imaging have not been obtained for the complete observed sample, the galaxies for which such data is missing must form an unbiased subset.

The final two criteria contrast the observed subsample for each cluster with the parent sample of spirals in the region. (4) We must have observed more than 10% of the parent cluster spiral population. (The parent sample is < 0.5 magnitudes deeper than the observed sample in completeness; see Paper III for an analysis of completeness in the observed dynamical subsample.) A case by case study of membership such as that done for the observed sample would have been very time consuming as there are more than 100 spirals in some of the clusters, so we have used the same constraints as in Figure 5 to define cluster membership for all parent sample galaxies in the vicinity of each cluster. The average fraction observed for the well sampled clusters is 29%, in line with our restriction to inclination angles greater than 30°. Note, however, the element of self-fulfilling prophecy, as the observed sample is always completely represented in the parent population, which in turn is sensitive to the depth to which the cluster region has been explored in redshift surveys. (5) The correlation between R distributions between the observed sample and the parent cluster spiral population must not be strongly biased, as compared to Monte Carlo simulations of randomly chosen subsamples of the same size.

The hatched region on each cluster plot in Figure 5 represents the spirals within our subsample; we can compare their distribution with that of the spiral fraction of the parent sample. We assume that the combined AGC and NED data provide a good representation of the complete population of spirals within the cluster, to within our magnitude limits, and compare the distribution of R within the dynamical subsample to it. The shape of the parent R distribution is frequently mirrored in the subsample, as in the case of A1656 and A539.

We have computed a correlation function between the R distribution of the parent and subsampled spirals within each cluster, as a function of R. The validity of the measured correlation is highly dependent upon the number of galaxies within each sample, so it is not enough to measure the correlation alone. We have run Monte Carlo trials on each cluster, sampling without replacement the parent set of spirals to form 100 randomly selected subsamples the same size as each observed subsample. We then compare the distribution of the correlation coefficients between the parent sample and each of the simulated subsamples, and the correlation for the observed subsample. Undersampled clusters were identified by a wide variation in the correlation of the simulated subsamples, and well sampled clusters were examined for signs of selection bias.

Clusters such as A426 and A262 were not sampled beyond a radius of 2 h^{-1} Mpc in the dynamics program, and thus the extreme outer envelope of parent spirals is undersampled at R ≥ 2.5. This is acceptable for our purposes, given our focus on the inner 2 h^{-1} Mpc. Three other clusters, however, show significant differences between parent and subsampled R distributions. The subsample for A2063 has a markedly different shape from that of the parent spiral population, particularly in the inner region. This is because the subsampling is very incomplete, and highly biased towards galaxies with strong 21 cm line profiles, in contrast to the other clusters. The clusters A779, A2147, A2152 and A2162 have not been sampled deeply enough and lack sufficient numbers in the observed sample. We thus discard all five from the dynamical program; they are not shown in Figures 1 through 3.

The remaining 13 clusters appear to have been well sampled, according to the above limits. The first two criteria have been relaxed slightly for A2666. It lies 4 h^{-1} Mpc from A2634 in a well sampled region, with many redshifts in the literature,

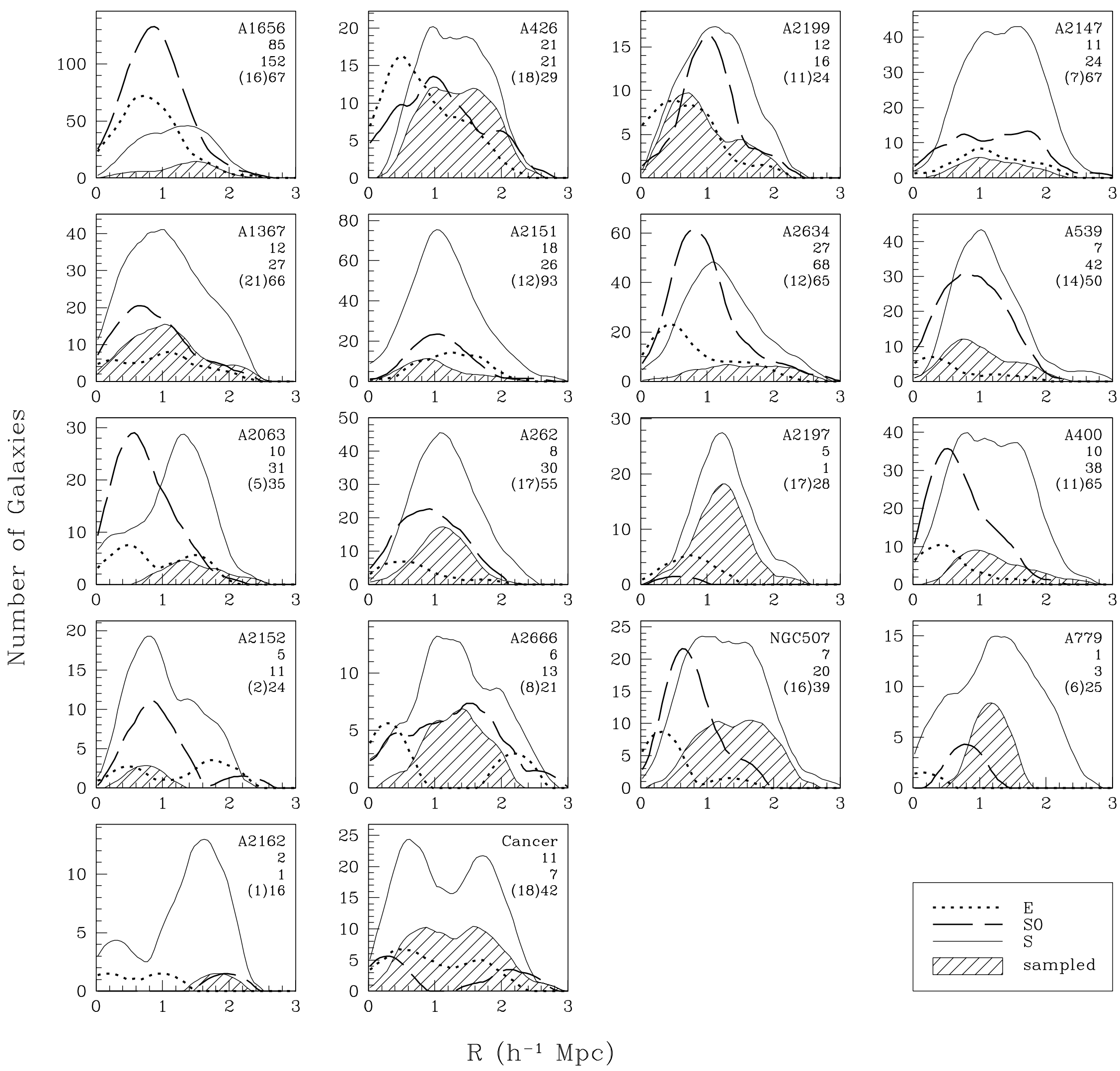

FIG. 5.— Distribution of the cluster offset, R, for galaxies of different morphological types within each cluster, ordered by X-ray temperature. Galaxies must fall within the inner $\frac{1}{2}$ h^{-1} Mpc and 5σ, or 2 h^{-1} Mpc and 3σ (relaxed to 6σ for Cancer and NGC 507), of the cluster to be included, and neighboring cluster contamination has been removed. The dotted line shows the distribution of ellipticals, the dashed line the S0s, and the solid line the spirals. The hatched areas show the subset of the parent spiral distribution targeted within our dynamical sample. The number of ellipticals, S0s, and spirals is indicated below the cluster name, with the number of spirals within our dynamical sample in parenthesis.

so we are confident that the parent spiral population is a good representation of the actual population in the region, down to our magnitude limits. Though we have observed only eight true cluster members they make up 38% of the spirals in the parent population of A2666, the expected fraction given our restriction in inclination angle. We thus assume that the small size of the observed sample reflects the limitation imposed by the small actual number of spirals within the cluster.

We lack H I line profiles for a significant number of galaxies within clusters A2151, A2197, and A2199, unlike the other well sampled clusters. Many of the galaxies in A2197 and A2199 were unreachable from Arecibo, and we did not have sufficient observing time to survey A2151; the galaxies without H I line profiles are not biased significantly (*i.e.* due only to the declination limit of the Arecibo dish for A2197 and A2199) relative to the observed sample. We have taken the precaution of conducting our analysis by including and then discarding the galaxies within these three clusters, and find no significant difference in the results.

3. DIRECT EVIDENCE FOR INFALL

The goal of our program is to explore the effects of the cluster environment on spiral galaxies. We have focused our efforts on two facets: (1) direct effects of infall on field spirals on a first pass towards the cluster core; (2) fundamental differences in the structure of cluster spirals relative to the field population, which could be caused either by perturbations from recent (or long-distant) infall, or by initial disk formation in a circumscribed, over-dense environment (*e.g.*, halo truncation). The combination of multiwavelenth observations spread across many clusters offers a complementary approach to higher resolution studies focussed on single clusters. We have obtained single-dish H I gas line profiles, moderate resolution major axis Hα and [N II] optical spectra, and photometric I-band images for our sample, augmented with B-band total magnitudes extracted as available from a variety of literature sources (primarily the RC3). We begin by identifying key observables within our data set which suggest a current or recent disturbance due to the cluster environment.

Albeit less individually illustrative, single–dish H I line profiles are observationally cheaper than two-dimensional H I maps and thus can be sampled in a wide range of environments as we have done here. The shapes of single-dish H I line profiles are sensitive to a number of factors unrelated to tidal interactions or gas stripping, including the inclusion of small, gas-rich companions within the telescope beam, high velocity clouds, and warps in the H I disk structure. However, the total H I gas mass is a key tracer of gas stripping, and, though crude, H I line profile shapes are still a powerful secondary indicator when used in conjunction with spatially resolved velocity profiles (see below).

The H I deficiency, as discussed in Paper I, is a measure of the difference between the measured H I mass and that expected for a galaxy of similar morphology and size. We divide our dynamical sample into an H I normal (gas-rich) population and an H I deficient (gas-poor) population, based on galaxy type and blue radius R_b correlations determined from a large body of field spirals (Solanes *et al.* 1996, 2001), where gas-poor spirals are deficient in H I by a factor of 2.5 or more (log H I $_{def} \geq 0.40$). Note that many cluster spirals as so deficient in H I gas that any remnant cannot be easily detected, and the quoted H I deficiency is an upper limit on the remaining gas mass based on instrumental sensitivity. In these cases, we have applied survival analysis to the observed upper limits (see Paper I).

Likewise, maps of the Hα as obtained from Fabry–Perot or fiber bundle techniques provide more detailed pictures of asymmetries but are relatively expensive to obtain. With their recognized limitations, we use spatially resolved Hα and [N II] optical spectra as primary indicators for infall-induced distortion. By evaluating the Hα flux distribution along the major axis rotation curves, we obtain a measure of the young star formation, and thus molecular gas and H II region strength across the entire disk. Our exposures are deep enough and the slit wide enough (20 - 40 h^{-1} pc) that the observed signal is spatially continuous rather than a series of isolated delta functions caused by individual H II regions entering the slit. It serves well as an estimate of the radial flux profile characteristic of the disk from one side to the other for such inclined galaxies.

Figure 6 shows the Hα, [N II], and H I data for a representative subset of our data set. By plotting our H I line profiles on the same velocity scale as the spatially resolved optical spectra, we can align the frequency distribution of H I gas to the spatial axis and estimate its distribution along the disk. For galaxies associated with a cluster, an arrow points towards the cluster center. As our sample is made up of fairly edge-on galaxies, a face-on encounter is suggested statistically when the arrow is perpendicular to the x-axis and an edge-on one when the arrow lies along the x-axis.

The optical spectra of galaxies in the field or more than 3 h^{-1} Mpc from the center of clusters (first two rows) share common properties of uniform shape and extent. They are symmetric when centered about the continuum or the median velocity, both in radial extent ($\sim$ 10 h^{-1} kpc), in radial strength, and in velocity structure. The shape of the rotation curves is moderately smooth, characterized by a steep inner rise, an elbow turnover point, and a relatively flat outer region. Both Hα and [N II] can be traced along the entire profile, except for the nucleus where the Hα may be partly absorbed. Large isolated H II regions can bias the small scale flux distribution, but the underlying structure is quite uniform. These galaxies have the expected amounts of H I gas, distributed in double-horned profiles. These objects define the *normal*, well-behaved appearance of optical rotation curves.

Most galaxies on the outskirts of all clusters, or located within cool (or not particularly rich) clusters display Hα flux characteristics similar to the field (UGC 927, in the third row, is representative). Most, though not all, contain the expected reservoir of H I gas. A small percentage display weak asymmetry in the distribution of Hα flux (fourth row). In these cases, we find that the truncated Hα distribution is matched by a decrease in the amount of equivalent velocity H I gas on that side of the disk.

In contract, galaxies with normal optical spectra are rarely found within the cores of rich, hot clusters. Instead, the spectra are less extended along the disk and exhibit a greater variation in line strength, and a greater difference between the small scale variations in velocity (*e.g.*, ripples) on the two sides of the rotation curve. A few, like UGC 6697 (row 3), show evidence for large-scale distortion in the shape of the velocity profile. The bulk of these Hα spectra divide into three categories. First, we find galaxies for which the distribution of Hα flux is truncated on one side of the disk, by at least either 5 h^{-1} kpc or 50%, relative to the other side. There is good agreement between the distribution of H I and Hα flux remaining in these *asymmetric* galaxies, which make up the bulk of the H I detections within hot clusters. Second, we find galaxies for which the Hα flux extends to less than either 5 h^{-1} kpc or 3 R_d across the entire disk. Third, we find galaxies for which there is no Hα emission detected across the disk at all. These galaxies are strongly H I deficient, with very few H I detections.

In summary, we define four classes based on Hα emission flux properties: (1) *normal*, showing properties equivalent to those found in the field, (2) *asymmetric*, with Hα flux truncated along one side of the disk, (3) *stripped*, with strong Hα truncation across the entire disk, and (4) *quenched*, with no Hα emission flux. These four terms will be italicized through the text, to avoid confusion with that used elsewhere. These classes can be closely compared to previous classification of cluster spirals (*i.e.* van den Bergh 1999 on anemic spirals; Cayatte *et al.* 1990, 1994, Guhathakurta *et al.* 1988 on the process of Virgo spiral infall), though we focus on the Hα distribution rather than that of H I. We have categorized infalling galaxies with different observables and are thus sensitive to different markers of evolution along the infall path, but classify the initial stages of infall (called *normal* here, analogous to Group I in Cayatte *et al.*) and the end-state (called *quenched* here, analogous to anemic, or to Group IV for Cayatte *et al.*) similarly.

Figure 7 shows a representative mosaic of I-band images of galaxies of all four classes. It appears that the underlying older stellar population has not been disturbed in any of these galaxies, and the processes which are stripping the gas and halting new star formation have not affected the distribution of the long-lived disk population. There are small variations in some of the *asymmetric* galaxies (A), but most display a normal I-band morphology. The *stripped* spirals (S) have a smooth distribution; some still show spiral arm structure. The *quenched* (Q) spirals rarely have strong spiral arm structure, though note the barred spiral UGC 1350. Our survey selection

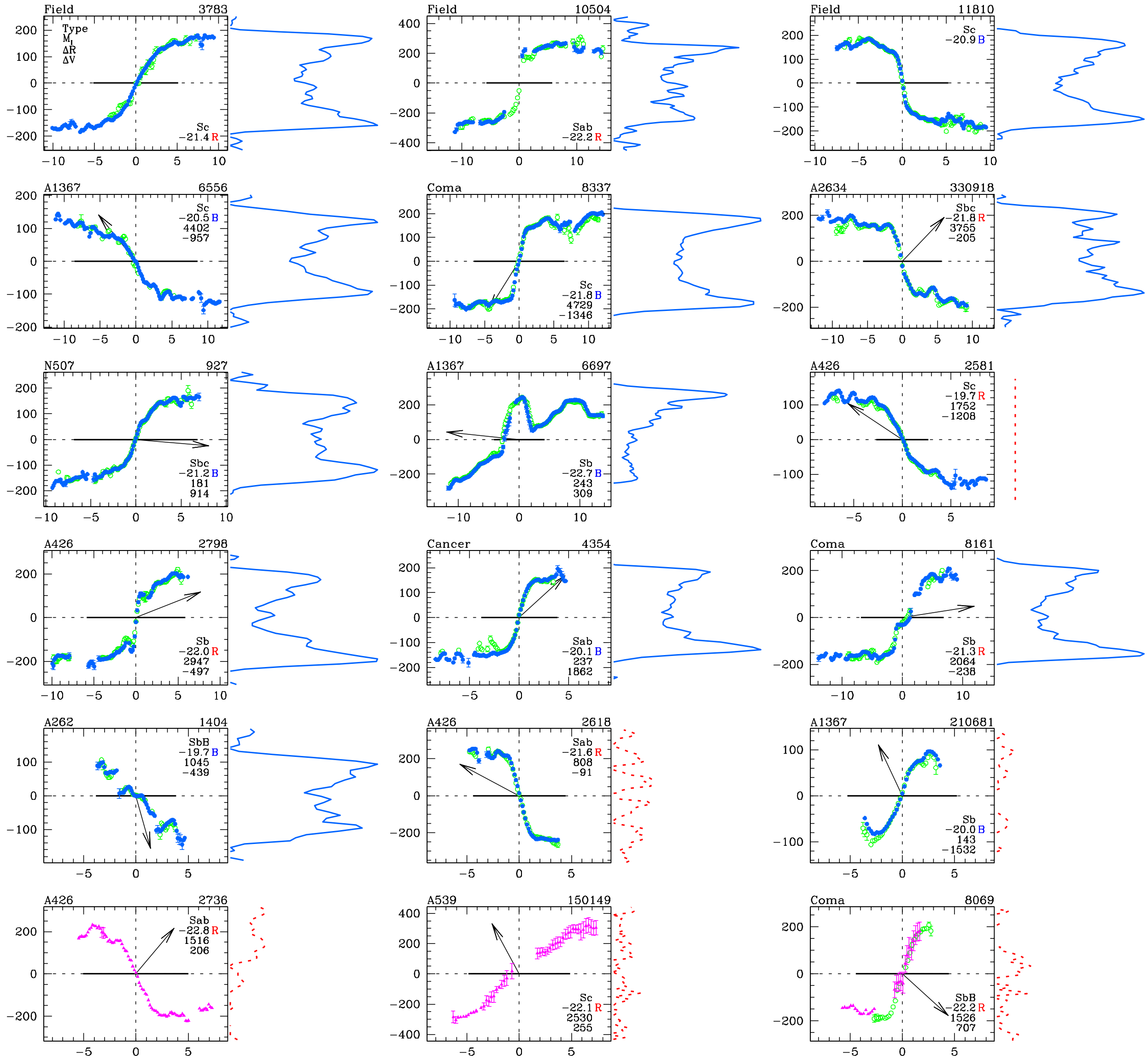

FIG. 6.— A representative mosaic of sets of three galaxies which are, row by row, (1) isolated in the field, (2) more than 3 h^{-1} Mpc from a cluster, (3) within 3 h^{-1} Mpc of a cluster, with *normal* Hα extent, (4) weakly asymmetric, (5) *stripped*, and (6) *quenched*. Boxes show the optical rotation curve (h^{-1} kpc on the x-axis, km s^{-1} on the y-axis, centered on the continuum) with the H I line profile to the right (counts on the x-axis and velocity on the y-axis, same scale as optical velocities). Hα emission flux is shown as blue solid circles, [N II] as hollow green circles, with error bars shown only where larger than 10 km s^{-1}, and Hα absorption as magenta triangles, with error bars shown only where larger than 20 km s^{-1}. H I flux is drawn with a blue solid line (HI normal) or a red dashed line (H I deficient). The peak H I flux is scaled to symbolize roughly the level of H I gas depletion; a linear H I flux indicates that we have a measurement of the total galaxy H I gas mass, but its distribution in radial velocity space is not available. A solid $\pm 2R_d$ disk length is drawn along the major axis, and an arrow points towards the cluster center. As our sample is made up of fairly edge-on galaxies, a face-on encounter is suggested statistically when the arrow is perpendicular to the disk and an edge-on one when the arrow lies along the disk. (Note that the angle between the arrow and the rotation curve means nothing!) Plots are annotated with galaxy type, M_I followed by B or R for blue or red B–I color, and clustercentric radius in h^{-1} kpc and velocity offset in km s^{-1}.

function discriminates against galaxies of an extremely disturbed morphology (not identifiable as spirals), in the process of a major merger (interacting with a companion), or undergoing extreme morphological transformation (*e.g.*, harassment). Because of this, we are not tracking evolutionary forces so strong as to significantly disturb the fundamental structure of the disk. Instead, we have focused upon galaxies which maintain a recognizable underlying form to the disk, allowing it to remain in place throughout the process of infall.

We suggest that these four Hα flux classes represent successive stages of the infall process, for relatively isolated, massive spirals interacting with a hot gas cluster component. Qualitatively, an incoming field spiral on the outskirts of a cluster will have the gas reservoir and star formation properties of a *normal* field spiral. Those which encounter the intracluster medium at a face-on orientation should be sieved of atomic gas across the outer region of the disk simultaneously, producing an abrupt halt to star formation due to the large cross-sectional interaction (*cf.* Abadi *et al.* gas stripping models). Those which enter the high density gas with a more edge-on orientation will be exposed to strong ram pressure forces on the leading edge of the disk, while the remainder of the gas

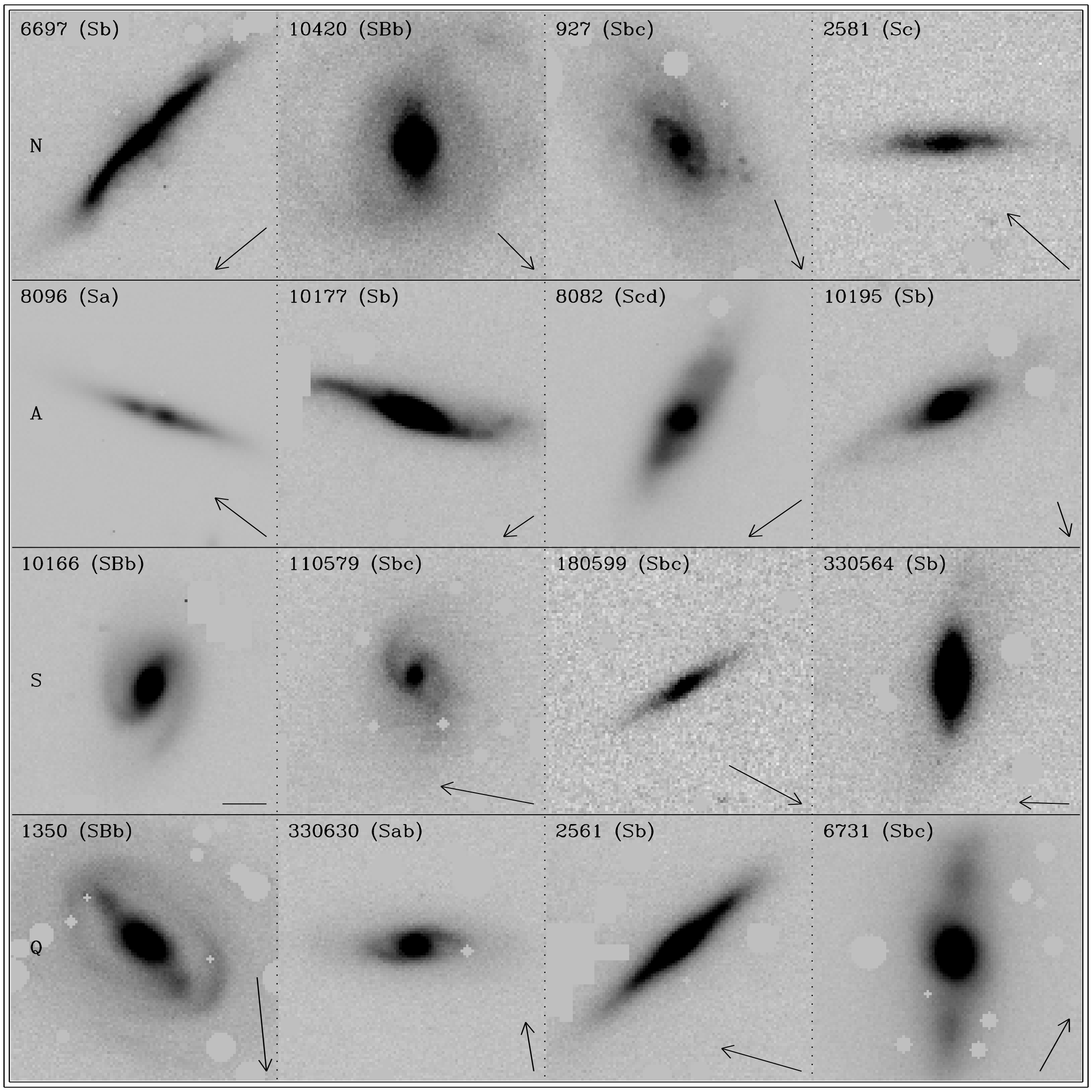

FIG. 7.— A representative *I*-band mosaic of four rows of Hα (1) *normal*, (2) *asymmetric*, (3) *stripped*, and (4) *quenched* spirals Postage stamps are each $1'$by $1'$, with north up and east to the left, and foreground stars have been masked. A 5 h^{-1} kpc bar shows the direction from the galaxy to the cluster center for all galaxies within 3 h^{-1} Mpc (all but UGC 10166). Some of the spirals are fairly edge-on and thus it can be difficult to assess the level of spiral arm structure, though the *quenched* barred spiral UGC 1350 suffers from no such ambiguities. The bulk of the *normal* spirals display smooth, regular morphology, though a few exceptions such as UGC 6697 and UGC 10420 can be found, mostly in the hot cluster cores. The *asymmetric* spirals show some distortion, consisting of variations in the ellipticity of the central surface brightness contours, disk contours off-center from the center of light, and some disruption in the outer disk, but fall mainly within the range observed within the *normal* spiral sample. The *stripped* and *quenched* spirals have smooth and regular surface brightness profiles.

reservoir will be sheltered for approximately half of a full disk rotation period, assuming a radial path of infall. The surprising detection of a significant number of galaxies with asymmetric distributions of H I and Hα flux suggests that the stripping process operates to quench star formation within 10^8 years, before the disk has rotated enough to erase directional signatures of infall. Recently stripped galaxies will maintain star formation in the central regions, of order 3 h^{-1} kpc in radius, where they have managed to retain a portion of the gas (possibly also funneled to the core in more violent cases of stripping). Young star formation will come to a halt across the disk, spiral structure will fade, and the galaxies will slowly drift towards the morphologies and orbital patterns of cluster S0s. This pattern falls broadly within the picture presented by models of infall (*cf.* Abadi *et al.* 1999; Vollmer *et al.* 2001b), including simulations of individual cases (*i.e.* Vollmer *et al.* 2001a), though detailed models include additional mechanisms to which our data are not sensitive (*e.g.*, bursts of star formation as stripped gas falls back onto the disk, Vollmer *et al.* 2001b). We do not attempt to constrain the gas stripping process with this level of detail, but identify a short-phase period based on observed Hα flux asymmetries which suggest a shorter timescale for ram pressure stripping to affect molecular gas and derivative star formation than is predicted by numerical simulations.

Figure 8 shows the spatial distribution of the spiral galaxies, within three h^{-1} Mpc of the clusters, employing symbols to distinguish different classes and Hα extents. Galaxies have

TABLE 2
DISTRIBUTION OF H I GAS PROPERTIES

Type	Field Galaxies					Cluster Members					Total	H I $_{gas}$ log(h^2 $M_\odot$)	B/T[a]	B–I (mags)
(1)	(2)[b]	(3)[c]	(4)[d]	(5)[e]	(6)[f]	(7)[b]	(8)[c]	(9)[d]	(10)[e]	(11)[f]	(12)	(13)	(14)	(15)
Normal (Hα emission consistent with isolated field)														
Sa – Sbc	31	4	0	0	0	67	13	6	1	17	139	9.43(0.43)	0.17(0.10)	1.90(0.42)
Sc – Sd	43	2	3	0	1	36	4	4	0	2	95	9.48(0.42)	0.07(0.06)	1.66(0.52)
Asymmetric (unequal Hα emission from one side of disk to the other)														
Sa – Sbc	0	0	0	0	0	3	0	3	0	2	8	9.18(0.51)	0.20(0.11)	1.94(0.58)
Sc – Sd	0	0	0	0	0	1	1	2	1	0	5	9.05(0.35)	0.20(0.15)	2.05(0.74)
Stripped (truncated Hα emission along disk)														
Sa – Sbc	0	0	0	1	0	1	5	3	0	2	12	8.64(0.38)	0.15(0.09)	2.02(0.56)
Sc – Sd	0	0	0	0	0	1	0	0	0	0	1	7.86	0.05	···
Quenched (Hα absorption along disk)														
Sa – Sbc	0	1	0	0	0	0	1	12	0	3	17	8.52(0.29)	0.20(0.10)	2.35(0.27)
Sc – Sd	0	0	0	0	0	0	0	4	0	0	4	8.52(0.14)	0.23(0.11)	···
Total														
Sa – Sbc	31	5	0	1	0	71	19	24	1	24	176			
Sc – Sd	43	2	3	0	1	38	5	10	1	2	105			
Sa – Sd	74	7	3	1	1	109	24	34	2	26	281			

[a]Bulge to total fraction of I-band luminosity
[b]HI-nrm: log $\mathrm{HI_{def}} < \log(2.5)$, detected H I normal galaxies
[c]HI-def: log $\mathrm{HI_{def}} \geq \log(2.5)$, detected H I deficient galaxies
[d]HI-lim: log $\mathrm{HI_{def}} \geq \log(2.5)$, from upper limit on H I gas
[e]HI-nol: upper limit on H I gas lies within HI-nrm range
[f]HI-non: H I content unknown

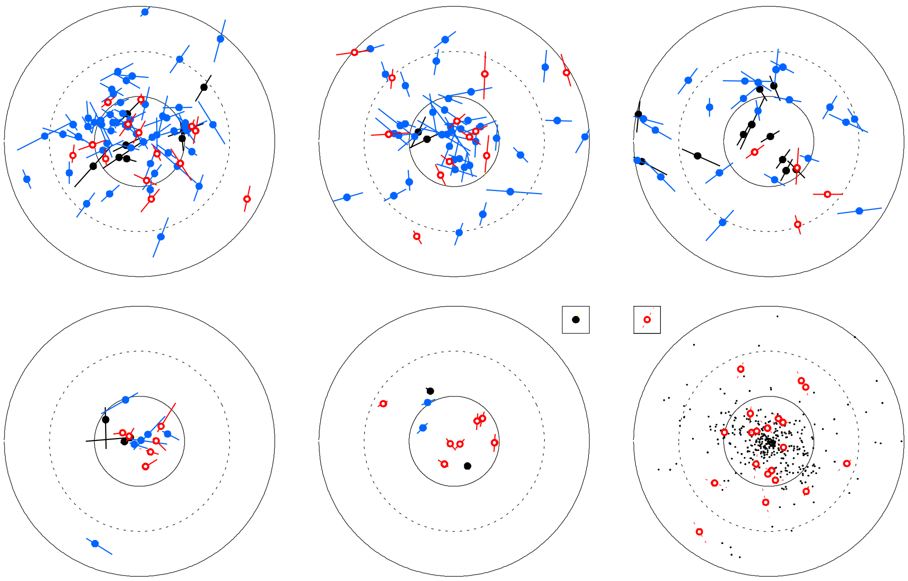

FIG. 8.— Distribution of galaxies within 3 h^{-1} Mpc of all clusters, with circles drawn at 1, 2, and 3 h^{-1} Mpc. H I normal galaxies are drawn in blue with solid bulges, HI deficient galaxies in red with hollow bulges, and galaxies of unknown H I gas mass in black with solid bulges. Individual galaxy glyphs show the extent of the Hα flux along the major axis of the disk; a solid line indicates Hα emission and a dashed line (lower right panel only) indicates Hα absorption. The upper panels show *normal* galaxies (no striking properties of Hα flux); on the right within A1656, A426, or A2199, in the middle within the remaining hot clusters A2151, A1367, A2634, and A539 and on the left within the cooler clusters. The lower left/middle/right panels show *asymmetric/stripped/quenched* galaxies. Boxed galaxies in the lower panels identify the two *stripped* or *quenched* galaxies beyond 3 h^{-1} Mpc. Cluster S0s have been added to the lower right panel as small black dots; their distribution peaks in the center and drops exponentially, while there are no quenched spirals in the inner 200 h^{-1} kpc of any of the clusters.

been divided into six categories, according to their Hα flux and the X-ray properties of their parent clusters. The top row contains all galaxies with *normal* Hα properties. From left to right, clusters are sorted into those with X-ray temperatures cooler than 3 keV, between 3 and 4.5 keV, and hotter than 4.5 keV. Both cool and warm clusters are characterized by a large population of H I normal galaxies and a smaller fraction of H I deficient ones; the radial galaxy distribution in all clusters peaks in the cores. The hottest clusters also contain galaxies with a range of H I gas masses, but those with *normal* Hα properties are found predominantly outside of the inner 600 h^{-1} kpc region. In summary, Hα *normal* galaxies are found throughout all of the clusters, but are scarce within the inner regions of the hottest cluster cores.

The bottom row shows the spatial distribution, from left to right, of *asymmetric*, *stripped*, and *quenched* spirals found in all of the clusters. Thirteen of the fourteen *asymmetric* galaxies are members of warm (above 3 keV) clusters. They are located preferentially in the inner 600 h^{-1} kpc region (the radial distribution differs from that of the *normal* galaxies found throughout the clusters at a >99% confidence level), where the effect of ram pressure stripping from the hot gas component is expected to become prevalent. Both strongly HI deficient, the *stripped* and *quenched* spirals exhibit a more relaxed radial distribution; we find them within clusters of all temperatures. The cores of the hottest clusters are thus shown to be populated predominantly with *asymmetric*, *stripped*, and *quenched* spirals, rather than those of the *normal* class. The remaining clusters contain galaxies with a range of Hα properties in the cores, but with a high *normal* fraction.

Table 2 summarizes the distribution of galaxies by class, HI content, cluster membership, morphological type and Hα extent. Within each class, galaxies are divided into early and late types; mean values of the H I mass, bulge–to–total luminosity and $B-I$ colors are also given. magnitudes from the RC3 where available or else from NED. Note that while the derived colors are imprecise, we use them only as a secondary indicator of star formation, binning the sample into wide color bins to identify galaxies with extreme colors. H I deficiency is more prominent within clusters, as expected, and also becomes stronger for galaxies without *normal* Hα flux. Both bulge fractions and $B-I$ colors appear to increase similarly, for *asymmetric* and *quenched* galaxies, while the situation for *stripped* galaxies is more complicated, as discussed below.

3.1. *Normal Spirals*

We have characterized the properties of the bulk of *normal* spirals as being equivalent to those found for field spirals. However, galaxies with *normal* Hα spectra within the inner regions (<900 h^{-1} kpc) of the hottest clusters within our sample tend to have a smaller Hα extent than expected (91% fall below the average value), and a lower Hα equivalent width. We lack H I measurements for a large number of these galaxies as they lie within the cluster A2199, but those which have been observed show extremely high H I deficiency.

In the inner 600 h^{-1} kpc region, where the hot X-ray gas component becomes significant and ram pressure stripping a serious concern, there are only five Hα *normal* galaxies found within A1656, A426, and A2199. Three lie on the 600 h^{-1} kpc outskirts and are oriented within 10° of a face-on trajectory relative to the cluster cores, suggesting a face-on infall path for a radial orbit. The remaining two are oriented more edge-on and have a maximum 6 h^{-1} kpc Hα extent, on the edge of our 5 h^{-1} kpc *stripped* criterion. These galaxies fit a picture in which no spiral passes through a hot core without substantial alteration.

Most galaxies within the cooler (kT $<$ 4 keV) clusters show far less evidence for substantial disruption. Many galaxies within the inner regions of A1367, A2151, A539, and A2634 display Hα *normal* spectra, with characteristics similar to those of the field. Those of moderately truncated Hα extent (25%) tend to be strongly H I deficient. There are seven galaxies, for example, with *normal* Hα spectra within 600 h^{-1} kpc of the core of A1367 (close neighbor to A1656), most with quite normal properties. We take special note, however, of UGC 6697, which has an extended but very disturbed rotation curve, characterized by very broad and strong Hα emission extending far beyond the nucleus. This well-studied object (Sullivan *et al.* 1981; Kennicutt, Bothun, & Schommer 1984, and references therein; Gavazzi *et al.* 2001) has a very high rate of star formation (EW$_{H\alpha}$ = 61Å), and the I-band image shows extreme distortion along the large edge-on disk, flaring at both ends. Nulson (1982) argued that the primary gas removal mechanism is turbulent viscous stripping rather than ram pressure, which would be inadequate to produce so strong an effect. More recently, Gavazzi *et al.* have combined narrowband Hα and broadband optical images with longslit observations taken at a variety of positions and position angles and Fabry-Perot interferometry and conclude that the object is composed of two interacting galaxies, the data for which are complicated by the presence of a superimposed galaxy lying directly in the background. Due to the presence of the background galaxy in the optical spectra, this object was not included when the *normal* sample was characterized (see Tables 2 and 3).

3.2. *Asymmetric Spirals*

It is well known that lopsidedness is a common feature in both the optical and HI disks of seemingly undisturbed galaxies (e.g., (Richter & Sancisi 1994; Rix & Zaritsky 1995; Kornreich, Haynes, Lovelace, & van Zee 2000). Weak trends in Hα extent and asymmetry with clustercentric radius were found for Hα strong detections in the nearby universe (Dale *et al.* 1999), though not for a similar sample of redshift $z \sim 0.1$ clusters (Dale & Uson 2003). The Virgo spiral NGC 4522 (Kenney & Koopmann 1999) is a clear case of a peculiar Hα flux distribution associated with ram pressure stripping across the disk of a galaxy. Indeed, moderate asymmetry, both dynamical and morphological, is common, occurring in 30% to 50% of galaxy disks located in a broad range of environments.

Here we use simple but robust criteria to distinguish the *asymmetric* spirals by quantifying the degree and extent of asymmetry observed in their Hα rotation curves. The determination of the extent is relatively insensitive to the specific detection criteria used when tracing the spectra, because the drop in signal to noise is quite abrupt (the spectra tend to terminate as a step function rather than gradually tapering off in intensity). A truncation in the radial extent of star formation is directly connected to an extreme curtailment of the gas reservoir. In contrast, the equivalent width of the Hα line flux is sensitive both to galaxy type and to extinction, and can be enhanced by some interactions (*e.g.*, UGC 6697, where gas funneled to the core is stimulating a starburst phase) or diminished by others.

In order to avoid asymmetry caused by a single isolated HII region or other peculiarity, we settled on two specific criteria for our *asymmetric* classification: the radial extents of Hα emission traced on each side of the disk must either differ by more than 5 h^{-1} kpc (Δ H$\alpha > 5$h^{-1} kpc) or form a ratio (r_1/r_2) of less than 1:2. The percentage of galaxies which met these criteria was less than 5% and all but one fall within 1 h^{-1} Mpc of a cluster core; the adopted criteria do indeed identify the extreme cases of asymmetry. Most of the 14 *asymmetric* spirals show a difference in Hα extent of less than 1:2, and for half of them this difference is also more than 5 h^{-1} kpc. In several cases the remaining Hα flux on the truncated side (within the

TABLE 3
MEAN PROPERTIES OF SPIRAL SUB-CLASSES

Population	ΔRadius (h^{-1} kpc)	Δcz (σ)	B/T	M_I (mag)	B–I (mag)	R_d (kpc/h)	R_b (h^{-1} kpc, R_d)		ORC[a]$_{ext}$ (h^{-1} kpc, R_d)		<DEF>	H I $_{gas}$ log(h^2 $M_\odot$)
(1)	(2)	(3)	(4)	(5)	(6)	(7)	(8)	(9)	(10)	(11)	(12)	(13)
Normal	1194(727)	1.0(1.4)	0.13(0.10)	-21.5(0.9)	1.81(0.47)	3.0(1.2)	13.0(4.5)	4.7(1.3)	9.9(3.5)	3.6(1.2)	0.09(0.33)	9.45(0.43)
Field	···	···	0.10(0.09)	-21.2(0.7)	1.74(0.44)	2.9(1.0)	13.6(2.9)	5.0(1.4)	10.8(3.1)	4.0(1.3)	0.00(0.23)	9.60(0.26)
Clusters	1194(727)	1.0(1.4)	0.14(0.10)	-21.5(0.9)	1.82(0.48)	3.0(1.3)	12.9(4.7)	4.6(1.3)	9.8(3.5)	3.6(1.2)	0.10(0.33)	9.42(0.43)
Early	1167(759)	1.1(1.2)	0.17(0.10)	-21.7(0.8)	1.90(0.42)	3.0(1.3)	13.1(4.5)	4.6(1.2)	9.8(3.7)	3.5(1.1)	0.10(0.32)	9.43(0.41)
Late	1357(681)	2.0(2.7)	0.07(0.06)	-21.1(0.8)	1.67(0.52)	2.9(1.1)	12.9(4.6)	4.8(1.4)	10.2(3.3)	3.8(1.3)	0.07(0.32)	9.48(0.42)
H I-nrm[b]	1265(728)	1.2(1.3)	0.13(0.10)	-21.5(0.9)	1.77(0.49)	3.0(1.2)	13.2(4.3)	4.7(1.3)	10.4(3.5)	3.7(1.2)	-0.03(0.20)	9.58(0.30)
H I-def[c]	951(486)	1.1(1.2)	0.15(0.11)	-21.4(1.0)	1.91(0.36)	2.6(1.1)	11.6(4.3)	4.9(1.2)	6.9(2.6)	3.1(1.2)	0.55(0.13)	8.91(0.25)
H I-lim[d]	1612(909)	3.3(4.2)	0.12(0.10)	-21.3(0.6)	1.84(0.32)	2.6(0.9)	12.5(4.2)	4.8(1.2)	8.5(2.5)	3.4(1.2)	0.90(0.25)	8.58(0.34)
Hot cores[e]	557(233)	1.1(0.6)	0.12(0.05)	-21.8(0.8)	2.01(0.36)	3.0(1.1)	12.3(5.0)	4.4(0.7)	8.0(3.7)	2.9(0.7)	0.29(0.30)	9.26(0.21)
Asymmetric	587(607)	1.0(0.7)	0.19(0.11)	-21.8(0.8)	1.97(0.58)	3.2(1.7)	13.5(5.4)	4.5(1.5)	10.5(6.0)	3.7(1.8)	0.41(0.46)	9.18(0.48)
B–I $\leq$ 1.5	473(178)	0.8(0.6)	0.09(0.06)	-21.2(0.8)	1.29(0.17)	2.1(1.1)	10.4(4.1)	5.3(1.7)	8.3(4.9)	4.5(2.4)	0.64(0.26)	8.84(0.27)
B–I $\geq$ 2.0	715(787)	1.0(0.7)	0.25(0.09)	-22.1(0.7)	2.31(0.35)	3.6(1.9)	13.6(5.0)	4.2(1.5)	10.2(4.9)	3.1(1.5)	0.25(0.47)	9.34(0.54)
Stripped	728(490)	1.6(1.5)	0.14(0.09)	-20.7(1.1)	2.02(0.56)	2.1(0.8)	9.2(3.1)	4.4(0.9)	4.1(0.9)	2.1(0.7)	0.74(0.37)	8.58(0.43)
Quenched	1019(609)	0.8(0.6)	0.20(0.10)	-21.9(0.5)	2.33(0.25)	2.3(0.5)	10.5(2.8)	4.8(1.4)	5.4(2.0)	2.7(0.7)	0.95(0.28)	8.52(0.20)

[a]The maximum extent of Hα, or of [N II] emission.
[b]log H I$_{def}$ < log(2.5).
[c]log H I$_{def}$ $\geq$ log(2.5).
[d]log H I$_{def}$ $\geq$ log(2.5), from upper limit on H I gas.
[e]Galaxies within clusters A1656, A426, and A2199, for which kT > 4 keV; within 900 h^{-1} kpc of the cores.

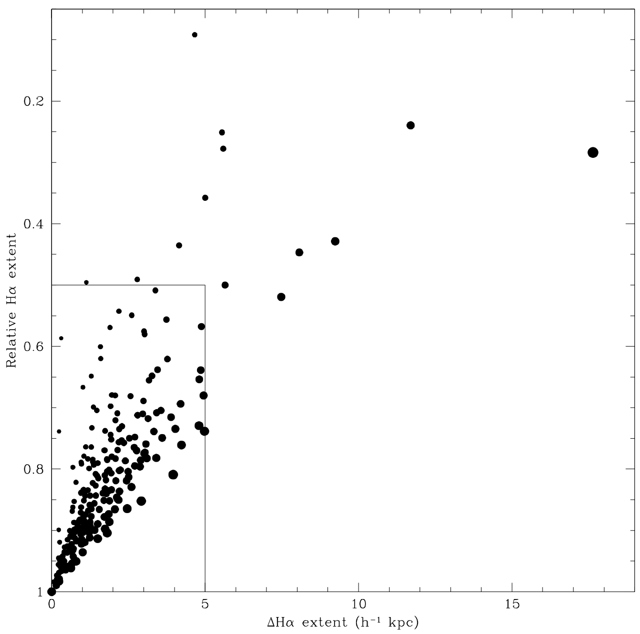

FIG. 9.— The distribution of Hα flux asymmetry indices throughout the sample. The x-axis shows the differential extent of Hα (longest – shortest radial extent, from one side of the disk to the other), and the y-axis the relative Hα extent (shortest over longest extent). Point size scales slightly with total Hα extent, and the most extended galaxies lie along the lower right-hand edge of the point distribution. The *asymmetric* galaxies fall outside of the locus in which most galaxies are found, bounded at a differential extent of 5 h^{-1} kpc and a relative extent of 50%. Most *asymmetric* galaxies fall beyond both limits, in the upper right-hand corner of the plot, and all have a relative extent less than 55%.

radius of truncation) is less strong than the flux on the other side of the nucleus at the same radius, but this is not a requirement. Figure 9 shows the distribution of the dynamic sample in terms of the two key asymmetry parameters. The *asymmetric* galaxies are clear outliers from the locus of the general distribution, along both parameter axes.

As discussed in Paper I, rotation curve centerpoints were determined by either balancing the two sides of the profile to determine a kinematic centerpoint, or by the spatial position of the center-of-light (COL) of the continuum. The *asymmetric* galaxies are preferentially COL-centered galaxies (four out of fourteen, or 29%, versus 12% for the complete sample). This is expected, as the kinematic measurement can be biased strongly when one side of the rotation curve is truncated, while the COL will remain unchanged. As an additional check, we folded the rotation curves about the centerpoints to verify that the inner profiles agreed on both sides of the nucleus. Figure 10 allows this check to be performed visually for the *asymmetric* sample; the selected centerpoints produce an acceptable match.

We note that while there are cases where [N II] but not Hα could be traced successfully through the nuclear region, there are few cases, primarily *asymmetric*, in which the [N II] flux extended to larger radius than the Hα flux. This is true for cases of both Hα emission, typically associated with strong [N II], and Hα absorption rotation curves, where [N II] can be difficult to detect at all at any radius. We elected to measure asymmetry purely from the Hα distributions, as the [N II] flux strength did not necessarily correlate with the Hα emission strength, and the increase in overall signal strength caused by the addition of the [N II] data would have been counterbalanced by a blurring of the most interesting spectra, where Hα flux was severely truncated.

Many spiral galaxies spread throughout the dynamical sample show a smaller difference in Hα emission extent, between 3 and 5 h^{-1} kpc. When we relaxed the 5 h^{-1} kpc criteria

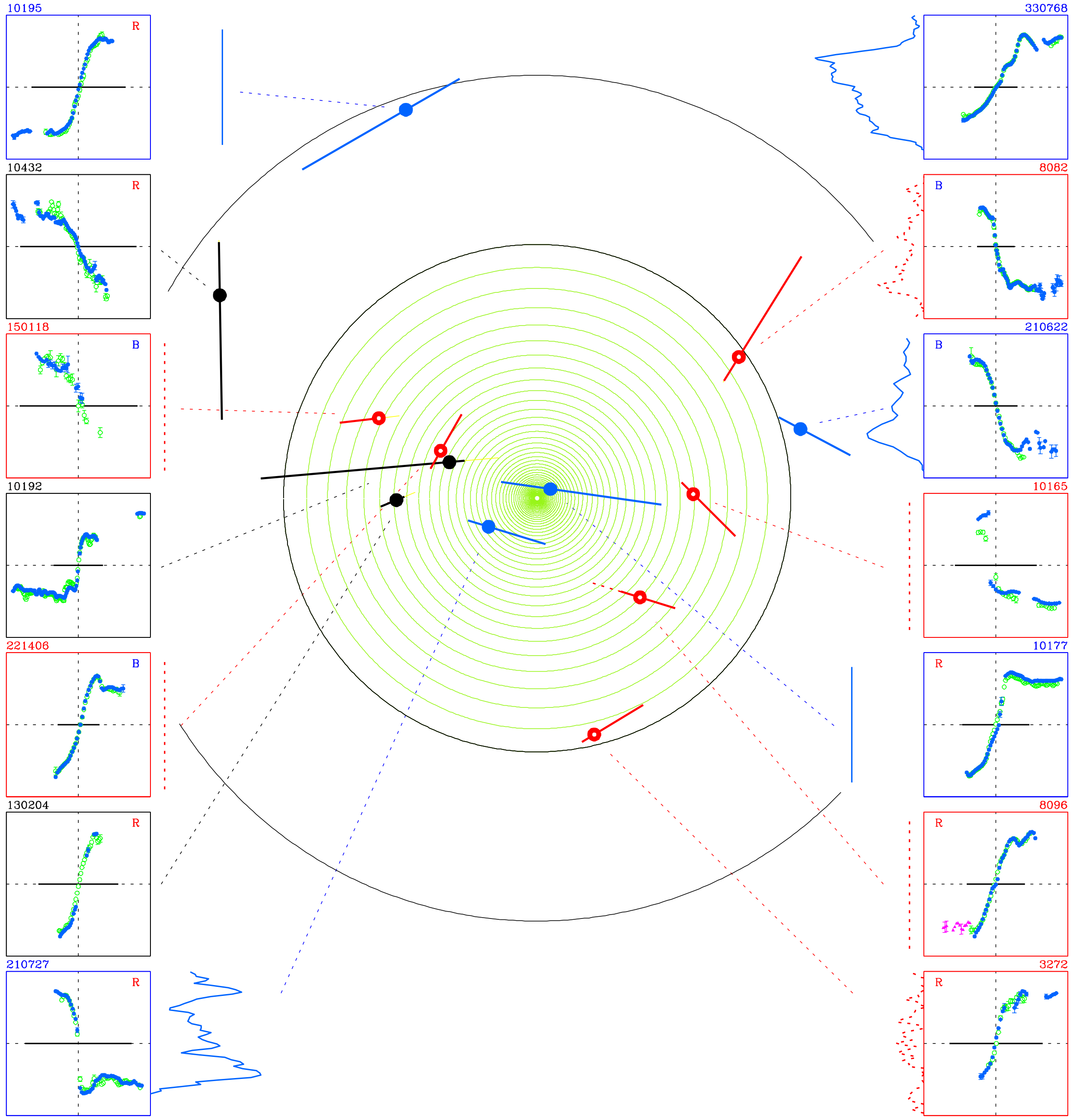

FIG. 10.— The spatial distribution of galaxies with *asymmetric* Hα flux extent. The outer circle is drawn at 1 h^{-1} Mpc and green mock hot X-ray gas contours fill the inner 600 h^{-1} kpc. Individual galaxy glyphs show the Hα flux along the major axis of the disk; a solid line indicates Hα emission, and a dotted line Hα absorption (UGC 8096/IC 3949 only). For UGC 10192 and AGC 130204/CGCG 540-115, the [N II] flux (yellow) extends beyond the Hα. Galaxies with normal amounts of H I are drawn in blue, while H I deficient galaxies are drawn in red (black for no H I data). Optical rotation curves and H I line profiles are shown as defined in Figure 6, and each galaxy is identified by its AGC number. The disks tend to point towards the cluster centers, suggesting edge-on rather than face-on infall into the hot gas. AGC 330768/CGCG 476-112 (upper right) is the sole *asymmetric* spiral found beyond 1 h^{-1} Mpc, within the envelope surrounding A2634. The disk of this five-armed, H I rich spiral is clearly disturbed, with a gigantic H II region at 5 h^{-1} kpc and a perturbing companion galaxy well within 20 h^{-1} kpc.

slightly, a large number of the additional, moderately asymmetric galaxies were found, many within the Cancer cluster. This suggests that less extreme forms of asymmetry may be a signature of loose group interactions, where the low relative velocities enable galaxy-galaxy interactions at an elevated rate.

We added a single galaxy (UGC 8096/IC 3949) to the *asymmetric* sample due to highly asymmetric Hα absorption flux. This reddened, H I deficient galaxy in the core of the Coma cluster exhibits Hα emission in the nuclear region and along one side of the disk, while the edge of the other side of the disk, pointing inwards towards the cluster core, shows only strong Hα absorption. UGC 8096/IC 3949 is the sole example of this pattern of extreme asymmetric Hα absorption within the dynamical sample.

Figure 10 illustrates the salient properties of these *asymmetric* galaxies. They have been drawn together into a single cluster diagram, offset from the centerpoint with the spatial offsets that they each have relative to their individual cluster centers. The contoured inner region extends from the cluster core to 600 h^{-1} kpc, an upper limit on where an infalling spiral could begin interacting significantly with the intracluster medium in a rich cluster. The complete dynamical sample extends to well beyond 2 h^{-1} Mpc for most of the sampled clusters, so these galaxies are clearly located preferentially in the cores.

AGC 330768/CGCG 476-112 is the sole *asymmetric* spiral found beyond 1 h^{-1} Mpc from a cluster core, located at a radius of 2.5 h^{-1} Mpc on the outskirts of A2634. This galaxy differs from the other *asymmetric* galaxies in several important respects: it is interacting with a companion which lies within 16 h^{-1} kpc, it is extremely gas-rich, with an H I deficiency measurement of -0.44, and its $B-I$ color places it in the center of the distribution for *normal* spirals. The cause of the asymmetry is clearly the current, large-scale interaction with a near neighbor; the *I*-band image shows a disturbed disk, with five arms and a gigantic H II region at a radius of 10 h^{-1} kpc which outshines even the nuclear continuum. The asymmetry is not caused directly by A2634, though the frequency of near neighbors is indirectly enhanced by the overdensity of galaxies, and groups of infalling galaxies, around the cluster.

The individual galaxy glyphs in Figure 10 have been drawn with a straight bar representing the *I*-band disk as if edge-on, where the bar length shows the extent of the disk in kiloparsecs and the relative length of the two sides shows the differing extent of the Hα flux on each side of the galaxy. We observe that the truncated sides of the disks tend to point inwards, along the direction that one would expect the galaxy to travel on a first infall path into the cluster core on a predominantly radial orbit. Observational evidence indicates that infalling H I deficient spirals tend to lie on radial orbits (Dressler 1986), and recent simulations of cluster dynamics (Moore *et al.* 1999) also find a preference for radial orbits within the spiral population, in support of such a pattern. For 8 of the 13 galaxies within the cores (we exclude outlier AGC 330768/CGCG 476-112) the truncated disk points toward the cluster core rather than away; this ratio rises to 8 out of 11 galaxies in the inner 600 h^{-1} kpc region. The median angle formed by the truncated side of the galaxy disks and the vectors pointing towards the center of the cluster is 43°, half of the 86° found for the *normal* spiral sample. This angle should lie near to 90° for a randomly oriented sample, and the probability of finding a mean value less than 45° is less than 0.2%.

Of the galaxies pointing away from the cluster centers, UGC 10195 and UGC 10432 are on the outskirts of the cores of warm clusters (radius $\sim$ 930 h^{-1} kpc), and UGC 10195 has both a normal H I gas mass and an apparent neighbor at 70 h^{-1} kpc. UGC 3272 and AGC 221406/IC 4040, with major axes almost perpendicular to the clustercentric vectors, have been considerably stripped of H I gas and may have recently passed through cluster centers to appear on the other side, and AGC 210727/CGCG 097-125 is a gas-rich spiral quite near to the center of A1367 (120 h^{-1} kpc, with a velocity offset of $+2\sigma$) which may be infalling into the cluster from the foreground. Without knowledge of the specific orbits of all of the *asymmetric* galaxies, we cannot claim that they show direct evidence for truncation on the leading edge of the disks, but the probability that the correlation between position and clustercentric angles is random is small.

Figure 10 also shows the Hα and H I flux for each galaxy. The Hα spectra have been centered within the display boxes from left to right, so that the continuum emission would lie at the center of each box if shown. A gap on one side of the box thus indicates that the Hα flux does not extend as far along that side of the disk as on the other side. Half of the truncated spirals are extremely H I deficient, while the remainder range from a factor of two in H I deficiency down to normal gas content. The average H I deficiency is greater than that of the normal spiral population by a factor of 1.75. H I fluxes have been plotted on the same velocity scale as the Hα rotation curves to demonstrate the relative amount of H I gas at each point along the disk, for detected galaxies. We observe that the truncated sides tend to show diminished H I flux, even within those spirals which still contain a normal amount of H I gas, in agreement with the trend for the weakly asymmetric galaxies as shown in Figure 6.

The asymmetric spirals are found predominantly within X-ray warm (kT $>$ 4 keV) clusters. Table 4 lists some of their key characteristics, in order of decreasing cluster X-ray temperature. Columns [14] and [15] contain the differential and relative extents of Hα emission flux, our quantified measures of asymmetry. Several exhibit extremely strong, broad nuclear emission, suggesting that a recent infusion of gas into the galaxy core may have stimulated a starburst phase. The galaxies have a bimodal distribution in $B-I$ above and below the mean color of the normal spirals (1.86), peaking at 2.43 (red, near to the color of the quenched spirals at 2.28) and at 1.42 (blue). These are the colors one would expect for a normal cluster spiral first entering a stimulated starburst phase (SB) and then reddening by $\sim$ 1 magnitude in a quiescent post-starburst phase (PSB).

The correlation between Hα maximum extent and truncation, and H I gas deficiency, is shown clearly in Figure 11. Early type asymmetric galaxies which still contain the bulk of the initial H I gas reservoirs are shifting down within the diagram towards the edge of the envelope in which H I normal spirals are found, though the maximum extent of Hα places them well within the normal distribution. Their H I deficient counterpoints have a maximum Hα extent which places them already at the edge of the envelope, and star formation is being suppressed across the remaining inner portion of the disk. The situation is more complicated for the few *asymmetric* late type spirals, which show extreme spatial truncation of star formation regardless of H I gas mass.

UGC 3272 and AGC 150118, like most of the spirals in the inner 1.5 h^{-1} Mpc of A539, are offset only a few hundred km s^{-1} from the cluster centroid velocity and fall well within the cluster dispersion (see Figure 3). The nuclear Hα emission for UGC 3272 is broad and strong, while AGC 150118 has extremely faint Hα and [N II] 6584Å; both are undetected in H I .

The remaining galaxies are divided between the clusters with fairly high X-ray luminosities. Two galaxies are drawn from the core of A1367. AGC 210727/CGCG 097-125 has broad and strong nuclear Hα emission, normal H I gas content, reddish color, and with a velocity offset of 2σ may be infalling from the foreground. AGC 210622/CGCG 097-062 is H I deficient by a factor of two, the distribution of the remaining H I gas clearly follows the spatial bias of the truncated Hα disk. The *I*-band image hints that the disk may be fainter on the truncated side, while more extended on the other

TABLE 4
PROPERTIES OF ASYMMETRIC SPIRALS

Cluster	Name	ΔRadius[a]	Δcz	Type	B/T	M_I	B–I	R_d	R_b	R_b	Optical Rotation Curve Extent[b]						<DEF>	H I $_{gas}$	$\Delta\Theta^c$
			(σ)			(mag)	(mag)			(R_d)					(R_d)	(R_d)		log(h^2 $M_\odot$)	(°)
(1)	(2)	(3)	(4)	(5)	(6)	(7)	(8)	(9)	(10)	(11)	(12)	(13)	(14)	(15)	(16)	(17)	(18)	(19)	(20)
A1656	AGC 221406/IC 4040[d]	248	0.83	Scd	0.07	-20.77	1.38	1.3	6.3	4.9	2.7	5.5	2.8	0.49	2.11	4.33	$\geq$ 0.51	$\leq$ 8.64	97
A1656	UGC 8082/NGC 4848	582	0.27	Scd	0.06	-22.09	1.50	2.2	15.7	7.1	3.7	15.4	11.7	0.24	1.75	6.93	0.78	9.02	23
A1656	UGC 8096/IC 3949[e]	305	0.58	Sa	0.25	-21.80	2.10	1.8	10.5	5.9	2.6	4.8	2.2	0.54	2.70	3.62	$\geq$ 0.71	$\leq$ 8.65	20
A426	AGC 130204/Z540-115	333	1.34	Sc	0.31	-21.67	2.91	2.5	7.7	3.2	1.1	2.2	1.1	0.49	0.96	1.09	$\geq$ 0.17	$\leq$ 9.27	21
A2151	UGC 10192[f]	230	-1.12	Sb	···	-22.33	···	4.6	14.5	3.2	7.0	24.6	17.6	0.28	1.51	5.33	···	···	31
A2151	UGC 10165	369	2.19	ScdB	···	···	···	···	24.2	···	2.2	7.7	5.6	0.28	···	···	$\geq$ 0.79	$\leq$ 9.40	47
A2151	UGC 10195	970	-0.40	Sb	0.35	-22.47	2.02	5.6	19.4	3.5	8.1	15.5	7.5	0.52	1.44	2.78	0.01	9.78	101
A2151	UGC 10177	38	-1.41	Sb	0.16	-23.42	2.10	3.7	17.8	4.8	6.5	14.6	8.1	0.45	1.74	3.90	-0.06	9.77	42
A1367	AGC 210622/Z097-062	644	1.75	Sb	0.04	-20.25	1.15	1.3	8.3	6.3	3.2	7.4	4.2	0.44	2.40	5.52	0.19	9.26	43
A1367	AGC 210727/Z097-125	133	2.27	Sc	0.34	-20.95	2.43	3.3	7.8	2.4	2.8	7.8	5.0	0.36	0.85	2.39	-0.01	9.43	133
A539	AGC 150118	419	-0.51	Sb	0.18	-21.73	1.15	3.6	11.4	3.2	0.5	5.1	4.6	0.09	0.74	1.42	$\geq$ 0.70	$\leq$ 8.80	34
A539	UGC 3272	575	0.51	Sb	0.11	-22.04	2.51	2.8	14.0	4.9	1.9	7.1	5.6	0.25	0.65	2.60	$\geq$ 0.85	$\leq$ 8.80	107
A2197	UGC 10432	891	1.06	Sb	0.31	-22.09	2.57	7.2	20.0	2.8	6.9	16.2	9.2	0.43	1.00	2.25	···	···	124
A2634	AGC 330768/Z476-112[g]	2478	0.24	Sb	0.15	-22.18	1.84	1.9	11.6	6.3	5.7	11.3	5.7	0.50	3.04	6.08	-0.44	9.98	82

[a] All length scales are expressed in units of h^{-1} kpc, unless explicitly stated otherwise.

[b] The minimum, maximum, and differential extent of Hα or [N II] emission followed by the ratio, and the minimum and maximum in units of R_d. Columns 14 and 15 contain the parameters used to define the asymmetry index.

[c] Angle between truncated side of disk and direction to cluster centerpoint.

[d] Bravo-Alfaro *et al.* (2000) report a detection in H I , with HI_{def} = 0.61, HI_{gas} = 8.52.

[e] Bravo-Alfaro *et al.* (2000) report a deeper observation in H I , with $HI_{def} \geq 1.9$, $HI_{gas} \leq 7.5$. Exhibits highly asymmetric Hα absorption flux (see Figure 10).

[f] Huchtmeier & Richter (1989) report a detection in H I .

[g] A five armed spiral, interacting with companion at 16 h^{-1} kpc. Note large H I gas mass.

side. Three more galaxies are found within A2151. The H I profile for UGC 10177 has been published previously (Figure 3 of Giovanelli & Haynes 1985). It shows more H I flux on the higher velocity side, in agreement with the optical rotation curve. The optical velocity map of Amram *et al.* (1992) further confirms the observed asymmetry in the Hα distribution. The *I*-band image suggests an increase in flux in front of the nucleus (as does that of UGC 8096/IC 3949). UGC 10165 is an extremely *asymmetric*, H I deficient galaxy in the core region, at a radius of 370 h^{-1} kpc. UGC 10192 has broad and extremely strong nuclear Hα emission. We have no H I data for the galaxy, but the strong, extended Hα emission suggests that the gas may still be present.

The last four galaxies are all H I deficient by more than a factor of six, and all lie within 600 h^{-1} kpc of the hottest cluster cores. Scd galaxies UGC 8082/NGC 4848 and AGC 221406/IC 4040 have blue colors and detectable remnants of H I gas, while the other two undetected galaxies have quite red $B-I$ colors. Spatially resolved H I maps for UGC 8082/NGC 4848 (Bravo-Alfaro *et al.* 2000) place the remaining H I gas aligned directly along the major axis and trailing the nontruncated side of the galaxy, which extends to 15 h^{-1} kpc and 7 R_d, with a perturbed H I gas distribution offset from the optical centroid by a considerable 8 h^{-1} kpc. The direction of the trailing wake of H I gas, and the correlation between Hα truncation and H I stripping, may support a radial orbit and edge-on infall path across the sky for this galaxy, located on the north-west edge of the cluster diffuse X-ray flux (Vikhlinin, Forman, & Jones 1997). The velocity offset of the galaxy from the cluster redshift is low (273 km s^{-1}) for its radius of 582 h^{-1} kpc, which suggests a large transverse velocity component of order 1,000 km s^{-1} and a corresponding timescale of 10^7 h^{-1} years since the onset of H I gas stripping. The timescale for the disturbance of molecular gas, and subsequent star formation suppression, on the truncated side of the disk would then be $\leq 5 \times 10^7$ h^{-1} years, half of a full disk rotation. However, Vollmer *et al.* (2001a) argue persuasively that this galaxy could not have experienced the observed amount of H I gas loss through ram pressure stripping without having passed through the center of the cluster, and have successfully simulated the distribution of the H I gas and Hα flux through re-accretion of atomic gas onto the disk. (In their model, a significant fraction of the stripped gas does not escape from the potential when stripped but falls back onto the disk, triggering a burst of star formation and explaining both the strong Hα flux and the blue colors.)

In contrast, AGC 221406/IC 4040 lies well with the projected diffuse X-ray gas component of A1656 (Vikhlinin, Forman, & Jones 1997). Though the galaxy is *asymmetric*, the maximum extent of Hα flux is 5.5 h^{-1} kpc, placing it just above the predicted stripping radius for a galaxy of this size (see Figure 11) and suggesting that gas stripping may have commenced throughout all four disk quadrants. The remaining H I gas lies again along the major axis (Bravo-Alfaro *et al.* 2000), supporting edge-on infall, though the galaxy projected location deep within the X-ray gas at a radius of 250 h^{-1} kpc and the concentration of H I gas along the more truncated Hα side of the disk suggest that this galaxy first encountered the intracluster medium more than a half rotational period ago (5 $\times$ 10^7 h^{-1} years). The large, positive velocity offset from the cluster redshift (+829 km s^{-1}), the small offset on the sky (4 h^{-1} kpc) between the remaining H I gas and the optical centroid, and the orientation of the Hα rotation curve (the side of maximum Hα extent rotates away from us, while the more

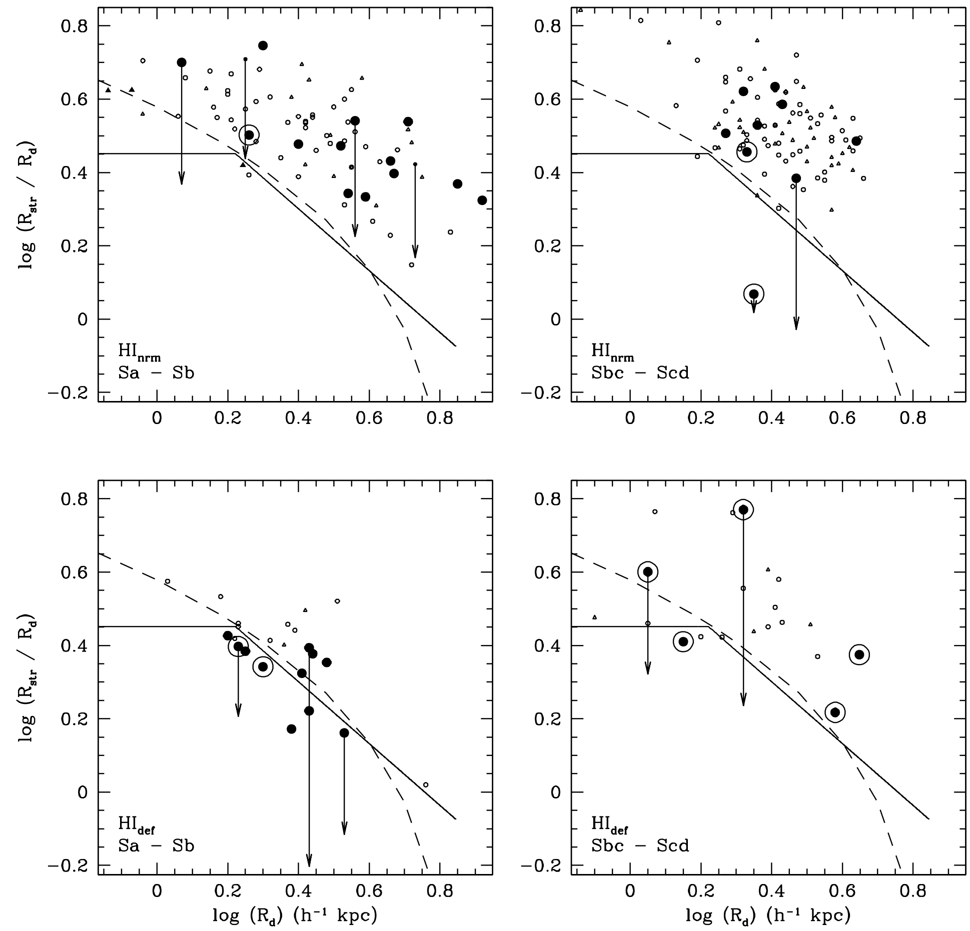

FIG. 11.— The radial stripping radius, the maximum extent of Hα and [N II] emission, as a function of disk scale length, divided into early **(left)** and late **(right)** types, and H I normal **(top)** and H I deficient **(bottom)** spirals. Maximum and minimum extents of Hα are connected with an arrow for *asymmetric* spirals. Small open triangles represent isolated field galaxies, and small open circles galaxies within cool clusters or located more than 900 h^{-1} kpc from the core of a warm (kT > 4 keV) cluster. Core members of warm clusters are shown with a large solid circle; those few within the cores of the three hottest clusters (A1656, A426, and A2199) are encircled. We have added as solid triangles in the upper left plot three early type Virgo spirals undergoing stripping taken from Cayatte *et al.* (1994), where the stripping radius has been determined from two-dimensional maps of the H I extent. The solid lines define our criterion for *stripped* spirals, and the dashed line a model stripping radius from Abadi *et al.* (1999).

truncated side comes towards us from out of the sky) suggest that this galaxy is falling into the cluster core from the foreground. Given this orientation and history, we cannot significantly constrain the timescales for gas stripping ($\geq 5 \times 10^7$ h^{-1} years) or star formation suppression.

AGC 130204/CGCG 540-115, at a similarly small radius within A426, has fairly weak Hα emission on the non-truncated side, which decreases by a factor of five in strength and becomes quite patchy, where detectable, on the truncated side (note, however, that [N II] 6584Å can be traced smoothly along both sides of the entire optical disk). UGC 8096/IC 3949 shows Hα in a fascinating combination of emission on one side, and a truncated absorption trough on the other, possibly a dynamic example of a later phase of the transition from spiral to S0. It is ranked as a post-starburst from its blue spectral features (Caldwell *et al.* 1999), and VLA H I observations (Bravo-Alfaro *et al.* 2001) limit the H I gas mass to $\leq 3 \times 10^7$ M$_\odot$.

We examined the clusters which showed large number of *asymmetric* members in detail, to see whether there were other candidate spiral galaxies in the core regions which ought to show asymmetry from interaction with the intracluster medium. The remaining galaxies in the inner 750 h^{-1} kpc were strongly H I deficient and appeared to have truncated Hα on both sides of the disk (see discussion in Section 3.3), indicating that they had already passed through the intracluster medium. Extending our search out to 900 h^{-1} kpc, we note the case of UGC 2617, the sole hot cluster core member offset significantly above the model stripping radius in Figure 11 which does not show signs of asymmetry. A large Sc galaxy located 858 h^{-1} kpc from the center of A426, UGC 2617 shows strong, extended Hα emission on both sides of the disk despite its high H I deficiency (H I $_{def}$ = 0.84). At this large a clustercentric radius, it is unlikely that the intracluster medium has caused the H I gas loss, as a first-pass galaxy would not yet have reached significant concentrations of hot gas and a full pass through the intracluster medium would have truncated the Hα emission for a galaxy of this morphological type; we suggest that its H I deficiency is unrelated to ram pressure stripping.

We further explored the remaining five A1656 galaxies within our dynamical sample also observed by Bravo-Alfaro *et al.* (AGC 221206/CGCG 160-058, UGC 8118, AGC 221409, UGC 8128/NGC 4911 and UGC 8140, all with *normal* Hα distributions) for evidence of ram pressure stripping. Four lie well to the north of the cluster X-ray gas and show strong H I gas, well-centered and extending beyond the optical disks. The fifth, UGC 8128/NGC 4911, located at a radius of 375 h^{-1} kpc, is a massive spiral with $M_I - 5$ log h = -22.5; Biviano *et al.* (1996) suggest that it is the dominant galaxy of a group which recently passed through the cluster core. The small offset between the optical and (deficient) HI gas mass centroids of 2-3 h^{-1} kpc *perpendicular* to the major axis, suggests a face-on infall path with gas stripping taking effect across the entire disk simultaneously (see also the velocity map derived in Amram *et al.* 1992). In summary, none are viable candidates for interaction with the intracluster medium and edge-on infall, suggesting that our Hα asymmetry criterion is identifying such galaxies as exist within the dynamical sample.

The *asymmetric* galaxies fall into two groups on the basis of optical colors, with $B-I$ colors either < 1.5 (blue) or $>$ 2.0 (red). The blue galaxies have the small B/T fractions of late type spirals, but are even bluer in $B-I$, have intrinsically smaller lengths of R_d, R_b, and Hα extent, and are profoundly H I deficient – suggestive of a central starburst phase stimulated by the gas stripping process. The red galaxies are larger and brighter and have B/T fractions higher than the mean of the early type (Sa through Sbc) galaxies in the sample. They have redder $B-I$ colors, range between normal and deficient amounts of H I gas, and the lengths of R_b and the Hα extent are slightly less *in units of* R_d, evidence of mild truncation of star formation in the outer regions of the disk. Taken together, the evidence supports a less extreme interaction with the intracluster medium, buffered by a low impact parameter and/or by the strength and shape of the potential well. These groups appear to be in two parallel, rather than sequential, phases along a single evolutionary path.

In summary, galaxies with asymmetric disk Hα flux, and a corresponding decrease in H I gas, can be found in a range of cluster environments, though concentrated in the hot X-ray gas cores of rich clusters. As these galaxies will be edge-on rather than face-on to the intracluster medium through which they fall, they should present a lower limit to the strength of the ram pressure stripping on the disk. Hα flux can be truncated on the side of the disk where the H I gas mass is slightly low but is not yet significantly depleted, indicating that the star formation is quite sensitive and responsive to changes in the localized gas mass. Both the red and the blue populations span the full range of H I deficiency, suggesting that the global instantaneous star formation rate is not a strong function of the available H I gas mass (in agreement with Bothun, Schommer, & Sullivan 1982, for cluster spirals, and as found for our total sample of normal spirals), and in fact the $B-I$ color correlates most strongly with spiral type.

The gas stripping could be caused by tidal forces, either from interaction with the cluster potential as the galaxy passes through the central core or from close (within 10 h^{-1} kpc) galaxy-galaxy interactions with other infalling spirals (Gnedin 2003a; also Abadi, Moore, & Bower 1999 whose models indicate that ram pressure stripping alone is insufficient to generate the observed stripping in larger spirals). However, the strong correlation between the orientation of the truncated side of the disk and the vector to the cluster core, the strong stripping of gas from the outer portions of the optical disk, and the spatial bias towards inner 600 h^{-1} kpc of the cluster (the maximum radius at which the hot gas should begin to strip gas within the richest clusters), and the lack of distortion in I-band disk surface brightness profiles suggests that ram pressure stripping is an important mechanism for suppressing star formation in these disks. The timescale for a full disk rotation, after which all quadrants of the disk would have rotated through the leading, exposed edge, is roughly one-tenth of a single pass through the intracluster medium at the core of a rich cluster. Coupled with the decrease in Hα flux and H I gas stripped from one side of the disk but no significant distortion of the disk in the I-band, this suggests that the stripping occurs on timescales well under 10^8 years. This is in agreement with predictions of star formation lifetimes based on star formation rates and H I gas masses (Kennicutt *et al.* 1984); note also that Abadi, Moore, & Bower (1999) predict that ram pressure stripping of H I gas will operate relatively quickly on a timescale of 10^7 years, significantly faster than galaxy-galaxy tidal interactions. The incidence of *asymmetric* galaxies, and timescale estimates derived above, suggest a current mass accretion rate of 100 h^3 $M_\odot$/year for the richest clusters. This is strikingly similar to the gas condensation rate from the intracluster medium, estimated from the measured excess central emission in cooling flow clusters (*e.g.*, Lufkin, Sarazin, & White 2000).

3.3. *Stripped Spirals*

What happens to *asymmetric* spirals after gas has been stripped from all disk quadrants? Their next evolutionary phase should last longer, as the abrupt suppression of wide-scale young star formation is followed by a slower decrease in the remaining star formation concentrated in the protected inner region (≤ 5 h^{-1} kpc) of the disk. Gas may not have been removed from this inner region, but the draining of the external reservoir insures that there will be little additional fuel funneled inwards in the future. Galaxies within this phase should be characterized by (a) young star formation confined to the inner few h^{-1} kpc across the entire disk, (b) H I deficiency, (c) warm cluster membership, and (d) a more relaxed orbital distribution than the *asymmetric* galaxies.

A fraction of infalling field spirals will exhibit these characteristics without passing through an *asymmetric* phase. Recent numerical simulations (Gnedin 2003a, 2003b; Moore *et al.* 1998) suggest that tidal forces, from a time-varying cluster potential or from galaxy-galaxy interactions (harassment), may be as important as ram pressure stripping in transforming spirals in cluster cores, and may operate more efficiently within infalling groups in the outer regions of clusters. Large spirals are predicted to experience halo truncation (beyond the optical radius), vertical heating resulting in a thickened disk, and tidal shocks leading to gas dissipation. The gas can lose enough angular momentum that it sinks to the galaxy nucleus (Barnes & Hernquist 1996) and fuels a starburst phase. In summary, face-on infall paths will strip the gas across the entire outer region of the disk simultaneously, more efficiently than edge-on interactions (Abadi, Moore, & Bower 1999), and mechanisms such as harassment or tidal interactions can remove the gas reservoir, on longer timescales.

We identify a candidate *stripped* population from the full dynamic sample, searching for galaxies with truncated star formation across the entire disk. These galaxies have a maximum extent of Hα flux of less than 5 h^{-1} kpc and of less than 3 R_d. Most are strongly deficient in H I gas. They are found in a more relaxed orbital distribution than the *asymmetric* galaxies, out to 2 h^{-1} Mpc from the cores of a wider range of clusters. In combination with their early morphological types and slightly reddened $B-I$ colors, this suggests that they are comprised of galaxies undergoing non-catastrophic stripping (*i.e.* no starburst phase, and still identifiable as spirals), and of formerly *asymmetric* galaxies which have penetrated the intracluster medium and continue along their orbital paths in a post-starburst phase.

Like the *asymmetric* galaxies, the *stripped* spirals were identified within the dynamical sample on the basis of Hα extent. The primary criterion is the truncation of Hα extent to within 5 h^{-1} kpc; the second limitation to within 3 R_d was added to eliminate the inclusion of unstripped galaxies with normal amounts of H I gas but with intrinsically small disk sizes. The *stripped* spirals are distributed along the extreme lower edge of the spatial distribution for all spirals, where H I deficient galaxies within the cores of hot clusters are located; relaxing the criteria would quickly result in the inclusion of galaxies which have normal amounts of H I gas, and are located in the field and in cooler clusters.

H I normal galaxies across the full range of environments within the dynamical sample lie within the same region well above the predicted stripping radius. The exceptions are the hot cluster core members (encircled on Figure 11), which follow the lower edge of the envelope. For early type, H I deficient galaxies there is a clear distinction between those located beyond the warm cluster cores well away from the intracluster medium, which still lie above the stripping radius, and those within the warm and hot cores, for which Hα is truncated to below the stripping radius. This environmental distinction is not reproduced for late type, HI deficient spirals.

Though the specific *stripped* criteria were motivated by the distribution of Hα flux throughout the dynamical sample, they agree fairly closely with model predictions which balance ram pressure stripping forces against the gravitational restoring force of the galaxy potential. Figure 11 shows good agreement between the two approaches, and the distribution of galaxies through the dynamical sample as a function of morphological type and H I gas deficiency. The extreme paucity of late type spirals within warm clusters is highlighted, and the lack of late type *stripped* galaxies suggests that infalling late type spirals are morphologically altered beyond recognition (Moore *et al.* 1996) or that star formation suppression in the outer regions of the disk leads to an early type classification (Koopmann 1997). There is a significant population of early type spirals within clusters of all temperatures. Those found within warm clusters follow the field and cold cluster distribution when their gas reservoirs are intact, though those within the hottest cluster cores fall along the lower edge. There is a clear distinction for H I deficient galaxies however, as the two populations begin to separate. The locus of cool cluster galaxies does not shift significantly, but those within warm clusters exhibit less extended Hα flux and tend to fall below the stripping radius. Early type galaxies within warm clusters are the only population found in this regime.

The *stripped* galaxies have a moderately tight radial distribution, more relaxed than the *asymmetric* galaxies but still fairly localized to the warm cluster cores, for which a crossing time is 10^9 years. This is a similar timescale to that of the *stripped* phase, given predictions from stellar population models and the strength of the Balmer features in spectra of post-starburst galaxies (1.5×10^9 years, *cf.* Poggianti & Barbaro 1996). One would thus expect 10 to 50 times more early type galaxies to appear in the *stripped* phase than the *asymmetric*, based on timescales alone and considering that some infalling galaxies will not pass through the *asymmetric* stage (*e.g.*, face-on infall paths). The fading expected in broadband colors is not sufficient to preferentially remove *stripped* galaxies from within our observational sample, but a significant decrease in blue light diameter R_b could force some below $30''$ in size (see discussion in Paper III), accounting for the relative counts of less than one to three.

3.4. *Quenched Spirals*

What happens to *stripped* galaxies after the remnants of young star formation along the entire disk slow to a halt, and there are no reservoirs of gas available for replenishment? Galaxy morphology, and star formation properties, should become dominated by the older, underlying stellar population. Our key tracer of star formation, Hα emission along the disk, fades into obscurity, to be replaced by an emerging Hα absorption feature characteristic of a stellar population dominated by A-type stars. We return to our complete dynamical sample, and examine the Hα flux characteristics throughout for evidence of such features. While the majority (93%) of the sampled galaxies exhibit strong Hα emission, the remaining 21 galaxies are characterized by a strong, extended absorption feature. We define them as *quenched* spirals. The Hα absorption trough is deep and can easily be traced through the nucleus and along the disk. It extends to a radius at or beyond 2 R_d for all but three of the galaxies. The *quenched* galaxies are extremely H I deficient (see Table 3), and $\frac{2}{3}$ have no detected H I gas at all.

Quenched spiral bulge fractions range from 20% to 60% and inclination angles from 45° to 90°, falling within the envelope of the complete dynamical sample. Nine of these galaxies are listed in the UGC (Nilson 1973), and for the remainder type codes were taken from another catalog (NGC , Dreyer 1888; IC , Dreyer 1895; CGCG , Zwicky *et al.* 1968) if available and determined from a visual examination of the POSS plates for the two previously uncataloged galaxies, before inclusion into the observing sample. Assigned type codes range from Sa through Sc, but are predominantly early types. Note the difficulty of typing the most edge-on portion of the sample; it can become problematical to assess the level of spiral arm structure, though one can look for dust lanes and signs of extinction.

We find the *quenched* spirals preferentially in the rich clusters A1656, A426 and A1367; the remaining half lie in the poorer clusters and none are found in Cancer or N507. Only one (UGC 11633, typed Sa) is from the field sample. These galaxies are situated as far out as a radius of 2.5 h^{-1} Mpc, quite beyond the cluster cores where spirals encounter both the intracluster medium and the enhanced tidal effects from close encounters and the cluster potential. This does not necessarily contradict formation through these mechanisms, however, as the very galaxy-galaxy interactions which lead to gas loss may also be responsible for redirecting the galaxies onto highly eccentric and loosely bound orbits (Balogh, Navarro, & Morris 2000). Their extreme H I deficiency indicates that the entire galaxy has been stripped, rather than just the outer regions of the disk. This suggests that tidal interactions, rather than ram pressure stripping which operates most efficiently in the outer disk, may be the key mechanism.

The simplest interpretation of the *quenched* galaxies is that they lie at a later stage along the transition from infalling field spirals to cluster S0s, passing or having already passed through a cluster core at least once. The dynamical sample was selected for spiral appearance with no deliberate inclusion of S0s. Any S0 contamination would thus come in the form of those which most closely resemble spirals rather than more spheroidal systems, and be the most likely candidates for reformed spirals within the S0 population. It is also clear that the *quenched* population cannot all be misclassified S0s, due to the cases of clear spiral arm morphology (*e.g.*, UGC 1350 within Figure 6). The relaxed orbital distribution, as shown in Figure 12, is completely different from that of the tightly centered S0 population.

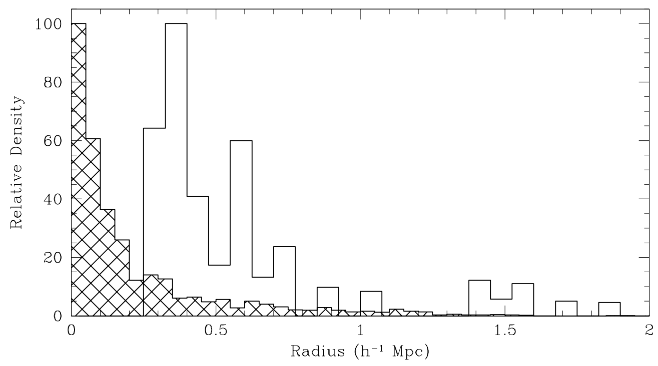

FIG. 12.— Radial distribution of *quenched* spirals (open) and of S0s (crossed), as a function of clustercentric radius. We find no *quenched* spirals within the inner 200 h^{-1} kpc of any of the clusters, where the S0 distribution peaks, and a Kolmogorov-Smirnov test estimates the probability of the two groups being drawn from different parent populations at greater than 96%.

These galaxies share certain characteristics with the population of E+A galaxies found in intermediate redshift clusters (Dressler & Gunn 1983) and locally in the field (Zabludoff *et al.* 1996) or post-starburst (PSB) galaxies in local clusters (Caldwell, Rose, & Dendy 1999). These designate galaxies which are characterized by (1) strong Balmer absorption lines, indicating an older stellar population of A-type stars and recent star formation, coupled with (2) an absence of emission lines (specifically, [O II] 3727Å) which rules out current star formation. Stellar population models suggest a recently ended ($\sim$ 1 Gigayear) burst of star formation, rather than the more constant rate of a typical spiral galaxy (Leonardi & Rose 1996). The finding of a significant population of field E+As, with evidence of tidal effects (Zabludoff *et al.* 1996), implies that these galaxies can manifest purely through galaxy-galaxy interactions. Their presence in rich clusters could then be attributed to previous interactions within an infalling group which left a signature, to tidal interactions within the cluster, or to cluster-specific mechanisms (*e.g.*, ram pressure stripping) if there exists more than one causative mechanism.

We lack the blue spectral coverage of [O II] 3727Å and Hβ, Hγ and Hδ necessary to make a full comparison with E+A spectra, our spectra being confined to a fairly narrow band around Hα, and our broadband coverage being restricted to $B-I$ colors. More importantly, we have selected for spiral galaxies while these samples have been focused upon elliptical and S0s (though Caldwell *et al.* 1996 find E+A galaxies which are determined to be disk systems). We have also selected highly inclined galaxies, in order to determine velocity widths, while the Caldwell *et al.* (1996) sample tends strongly towards face-on galaxies for which the structure and stellar populations can be more easily examined. Though we both have surveyed the Coma cluster, there is thus little overlap (though see discussion of UGC 8096/IC 3949 in Section 3.2) between our observational samples. Nonetheless, it is possible that our quenched spirals represent an evolved form of late type E+A galaxies, as the bulk of the PSB galaxies do for early types.

4. CONCLUSIONS

A strong inverse relation is obtained between the fraction of spirals and that of S0s, within the inner 1 h^{-1} Mpc or including infalling groups of spirals within up to 2 h^{-1} Mpc in local cluster membership calculations. The elliptical fraction, in contrast, holds fairly constant across the full range of three orders of magnitude in cluster X-ray luminosity. We have explored the strong correlation between H I gas stripping and the consequential suppression of young star formation, finding a correlation between the distribution of H I flux and of H II regions within the galaxy disks. To this end, we have divided the sample into four groups, on the basis of Hα emission properties.

Group I: *normal* spirals, with no particularly striking properties in the extent and strength of the observed Hα emission flux. Many, but not all, of these spirals have the expected amount of atomic gas for their optical size and morphological type. Most of the field spirals fall into this category, and the cluster spirals which do so tend to have similar properties as the field galaxies. This group also includes a small number of spirals located in the cores of rich clusters with patchy, somewhat decremented Hα emission flux extent. They appear to be infalling at a face-on orientation into the intracluster medium, and the gas reservoir is being stripped simultaneously across the entire radial extent of the disk.

Group II: *asymmetric* spirals, where the radial extents of Hα emission traced on each side of the disk either differ by more than 5 h^{-1} kpc or form a ratio of less than 1:2. Galaxies with this degree of asymmetry are not observed beyond 1 h^{-1} Mpc in any of the clusters, and are found predominantly in the richest cluster cores. Half are deficient in H I , with an upper limit of 30% of the expected H I gas, and the distribution of detected H I gas correlates with that of the Hα emission. They are oriented preferentially edge-on to the cores, with truncation of Hα flux *and* H I flux along the leading edge, suggesting that ram pressure stripping from a first pass through the intracluster medium plays an important role in generating this effect. The suppression of star formation along the disk occurs on a timescale similar to that of the H I gas stripping, as we find many galaxies where the gas stripping process has begun (low H I gas content and asymmetry in the two-horn H I line profile) but not yet been completed (a substantial amount of H I gas remains) where star formation has already been terminated along the leading edge of the disk.

The *asymmetric* galaxies fall into two groups, with $B-I$ colors either $<$ 1.5 (blue) or $>$ 2.0 (red). The blue galaxies have the small B/T fractions of late type spirals, but are even bluer in $B-I$, have intrinsically smaller lengths of R_d, R_b, and Hα extent, and are profoundly H I deficient – suggestive of a central starburst phase stimulated by the gas stripping process. The red galaxies are larger and brighter and have B/T fractions higher than the mean of the early type (Sa through Sbc) galaxies in the sample. They have redder $B-I$ colors, range between normal and deficient in H I , and the lengths of R_b and the Hα extent are slightly less *in units of* R_d, evidence of mild truncation of star formation in the outer regions of the disk. Taken together, the evidence supports a less extreme interaction with the cluster, supported perhaps by a low impact parameter or by the greater resistive force of a more massive potential well. These two groups appear to be on parallel, rather than sequential, tracks in their morphological histories.

Group III: *stripped* spirals, where the extent of Hα emission is less than 5 h^{-1} kpc on both sides of the disk and extends to less than 3 disk scale lengths. The bulk of these galaxies are strongly deficient in H I . They are found in a more relaxed orbital distribution than the *asymmetric* galaxies, out to 2 h^{-1} Mpc from the cores of a wider range of clusters. In combination with their slightly reddened colors, this suggests that they are comprised of less massive systems currently undergoing non-catastrophic stripping (*i.e.* no starburst phase, and still identifiable as spirals), and of blue *asymmetric* galaxies which have already passed through the cores and are now in a post-starburst phase.

Group IV: *quenched* spirals, for which star formation has been halted across the entire disk and Hα is found only in absorption. These galaxies range in appearance between possible edge-on S0s, and (primarily early type) spirals with clear spiral arm structure. They are 1 magnitude fainter in I-band than early type H I normal field spirals, 0.5 magnitudes redder in $B-I$, their disk scale lengths are a factor of 2 smaller, and the extent of the stellar Hα (absorption) flux is quite truncated along the disk (relative to the normal Hα extent). H I observations place an upper limit of one-tenth of the expected H I flux on the sample, and 90% are undetected. These galaxies may serve to illustrate the transition stage of a morphological transformation between infalling field spiral and cluster S0s. Their current orbital distribution is far less radially concentrated than that of present day S0s, and on a timescale of a few Gigayears they may slowly blend with that population.

In the richest, hottest clusters we find primarily *asymmetric, stripped,* and *quenched* galaxies, and *normal* edge-on infalling spirals within 1 h^{-1} Mpc of the cores. Less rich clusters contain primarily *normal* spirals, at all radii. This is consistent with a picture of infalling spirals being significantly altered by ram-pressure stripping in the hot cores, while galaxy-galaxy interactions and tidal forces play a role throughout the entire cluster distribution, and at larger radii.

In summary, we have explored the formation and evolution of spiral galaxies in local clusters through a combination of optical and H I properties. We find a clear relationship between H I gas stripping and the consequential suppression of young star formation; both occur quickly within spirals infalling into an intracluster medium of hot gas. We have traced galaxies through a progression of infall stages, beginning with infalling field spirals and transforming via gas stripping and passive fading into cluster proto-S0s (not with a bang but a whimper).

5. ACKNOWLEDGMENTS

The data presented in this paper are based upon observations carried out at the Arecibo Observatory, which is part of the National Astronomy and Ionosphere Center (NAIC), at Green Bank, which is part of the National Radio Astronomy Observatory (NRAO), at the Kitt Peak National Observatory (KPNO), the Palomar Observatory (PO), and the Michigan–Dartmouth–MIT Observatory (MDM). NAIC is operated by Cornell University, NRAO by Associated Universities, inc., KPNO and CTIO by Associated Universities for Research in Astronomy, all under cooperative agreements with the National Science Foundation. The MDM Observatory is jointly operated by the University of Michigan, Dartmouth College and the Massachusetts Institute of Technology on Kitt Peak mountain, Arizona. The Hale telescope at the PO is operated by the California Institute of Technology under a cooperative agreement with Cornell University and the Jet Propulsion Laboratory. We thank the staff members at these observatories who so tirelessly dedicated their time to insure the success of these observations.

We also thank Sc project team members John Salzer, Gary Wegner, Wolfram Freudling, Luiz da Costa, and Pierre Chamaraux, and also Shoko Sakai and Marco Scodeggio, for sharing their data in advance of publication. Mario Abadi kindly provided the output data from a ram-pressure stripping model, and Danny Dale provided tabulated data in electronic form. N.P.V. is pleased to thank Ann Zabludoff and Sandra Faber for many enlightening discussions regarding cluster formation, and Karl Gebhardt for generously sharing his adaptive kernel density fitting routines. The text of this manuscript was much improved by careful reading on the part of Richard Ellis. We thank the anonymous referee for helpful comments on the manuscript.

N.P.V. is a Guest User, Canadian Astronomy Data Center, which is operated by the Dominion Astrophysical Observatory for the National Research Council of Canada's Herzberg Institute of Astrophysics. This research has made use of the NASA/IPAC Extragalactic Database (NED) which is operated by the Jet Propulsion Laboratory, California Institute of Technology, under contract with NASA, and NASA's Astrophysics Data System Abstract Service (ADS). This research was supported by NSF grants AST92–18038 and AST95–28860 to M.P.H. and T.H., AST90–23450 to M.P.H., AST94–20505 to R.G., and NSF–0123690 via the ADVANCE Institutional Transformation Program at NMSU, and NASA grants GO-07883.01-96A to N.P.V. and NAS5–1661 to the WFPC1 IDT. N.P.V. acknowledges the generous support of an Institute of Astronomy rolling grant from PPARC, reference number PPA/G/O/1997/00793.

REFERENCES

Abadi, M. G., Moore, B., & Bower, R. G. 1999, MNRAS, 308, 947
Abell, G. O., Corwin, H. G., Jr., & Olowin, R. P. 1989, ApJS, 70, 1
Abramopoulos, F., & Ku, W. H. M. 1983, ApJ, 271, 446
Amram, P., Le Coarer, E., Marcelin, M., Balkowski, C., Sullivan, W. T., III, & Cayatte, V. 1992, A&AS, 94,175
Amram, P., Sullivan, W. T., III, Balkowski, C., Marcelin, M., & Cayatte, V. 1993, ApJ, 403, L59
Andreon, S. 1998, ApJ501,533
Balogh, M. L., Navarro, J. F., & Morris, S. L. 2000, ApJ, 540, 113
Barmby, P., & Huchra, J. P. 1998, AJ, 115, 6
Balogh, M. L., Schade, D., Morris, S. L., Yee, H. K. C., Carlberg, R. G., & Ellingson, E. 1998, ApJ, 504, L75
Barnes, J. E., & Hernquist, L. 1996, AJ, 471, 115
Bautz, L. P., & Morgan, W. W. 1970, ApJ, 162, L149
Bird, C. M., Dickey, J. M., & Salpeter, E. E. 1993, ApJ, 404, 81
Biviano, A., Durret, F., Gerbal, D., Le Fèvre, O., Lobo, C., Mazure, A., & Slezak, E. 1996, A&A, 311, 95
Bothun, G. D., Geller, M. J., Beers, T. C., & Huchra, J. P. 1983, ApJ, 268, 47
Bothun, G. D., Schommer, R. A., & Sullivan, W. T., III 1982, AJ, 87, 731
Bravo-Alfaro, H., Cayatte, V., van Gorkom, J. H., & Balkowski, C. 2000, AJ, 119, 580
Bravo-Alfaro, H., Cayatte, V., van Gorkom, J. H., & Balkowski, C. 2001, A&A, 379, 347
Bravo-Alfaro, H., Szomoru, A., Cayatte, V., Balkowski, C., & Sancisi, R. 1997, A&AS, 126, 537
Butcher, H. R., & Oemler, A., Jr. 1978, ApJ, 226, 559
Caldwell, N., Rose, J. A., & Dendy, K. 1999, AJ, 117, 140
Caldwell, N., Rose, J. A., Franx, M., & Leonardi, A. J. 1996, AJ, 111, 78
Cayatte, V., Balkowski, C., van Gorkom, J. H., & Kotanyi, C. 1990, AJ, 100, 604

Cayatte, V., Kotanyi, C., Balkowski, C., & van Gorkom, J. H. 1994, AJ, 107, 1003
Couch, W. J., & Sharples, R. M. 1987, MNRAS, 229, 423
Couch, W. J., Ellis, R. S., Sharples, R. M., & Smail, I. 1994, ApJ, 430, 121
Cowie, L. L., & Songaila, A. 1977, Nature, 266, 501
Dale, D. A., Giovanelli, R., Haynes, M. P., Hardy, E., & Campusano, L. E. 1999, AJ, 118, 1468
David, L. P., Slyz, A., Jones, C., Forman, W., Vrtilek, S. D., & Arnaud, K. A. 1993, ApJ, 412, 479
Dale, D. A., Giovanelli, R., Haynes, M. P., Hardy, E., & Campusano, L. E. 2001, AJ, 121, 1886
Dale, D. A., & Uson, J. M. 2003, AJ, 126, 675
de Vaucouleurs, G., de Vaucouleurs, A., Corwin, H. G., Jr., Buta, R. J., Paturel, G., & Fouque, P. 1991, Third Reference Catalogue of Bright Galaxies, Vol. 1-3 (Berlin: Springer–Verlag) (RC3)
Distefano, A., Rampazzo, R., Chincarini, G. L., & de Souza, R. 1990, A&AS, 86, 7
Dressler, A. 1980a, ApJ, 236, 351
Dressler, A. 1980b, ApJS, 42, 565
Dressler, A. 1986, ApJ, 301, 35
Dressler, A., & Gunn, J. E. 1983, ApJ, 270, 7
Dressler, A., *et al.* 1997, ApJ, 490, 577
Dreyer, J. L. E. 1888, MmRAS, 49, 1 (NGC)
Dreyer, J. L. E. 1895, MmRAS, 51, 185 (IC)
Ebeling, H., Voges, W., Bohringer, H., Edge, A. C., Huchra, J. P., & Briel, U. G. 1996, MNRAS, 281, 799
Edge, A. C. & Stewart, G. C. 1991, MNRAS, 252, 428
Ellis, R. S., Smail, I., Dressler, A., Couch, W. J., Oemler, A., Jr., Butcher, H., & Sharples, R. M. 1997, ApJ, 483, 582
Fasano, G., Poggianti, B. M., Couch, W. J., Bettoni, D., Kjaergaard, P., & Moles, M. 2000, ApJ, 542, 673
Fisher, D., Franx, M., & Illingworth, G. 1996, ApJ, 459, 110
Forbes, D. A., & Whitmore, B. C. 1989, ApJ, 339, 657
Gavazzi, G., Marcelin, M., Boselli, A., Amram, P., Vílchez, J. M., Iglesias-Paramo, J., & Tarenghi, M. A&A, 377, 745
Ghigna, S., Moore, B., Governato, F., Lake, G., Quinn, T., Stadel, J. 1998, MNRAS, 300, 146
Giovanelli, R., & Haynes, M. P. 1985, ApJ, 292, 404
Giovanelli, R., Haynes, M. P., Herter, T., Vogt, N. P., Wegner, G., Salzer, J. J., da Costa, L. N., & Freudling, W. 1997, AJ, 113, 22
Gnedin, O. Y. 2003a, ApJ, 582, 141
Gnedin, O. Y. 2003b, ApJ, 589, 752
Guhathakurta, P., van Gorkom, J. H., Kotanyi, C. G., & Balkowski, C. 1988, AJ, 96, 851
Gunn, J. E., & Gott, J. R., III 1972, ApJ, 176, 1
Huchtmeier, W. K. & Richter, O.-G. 1989, A&A, 210, 1
Jones, L., Smail, I., & Couch, W. J. 2000, ApJ, 528, 118
Kenney, J. D. P., & Koopmann, R. A. 1999, AJ, 117, 181
Kennicutt, R. C., Jr., Bothun, G. D., & Schommer, R. A. 1984, AJ, 89, 1279
Kent, S. M., & Gunn, J. E. 1982, AJ, 87, 945
Kent, S. M., & Sargent, W. L. W. 1983, AJ, 88, 697
Kodama, T., & Bower, R. G. 2001, MNRAS, 321, 18
Kodama, T., & Smail, I. 2001, MNRAS, 326, 637
Koopmann, R. A. 1997, Ph.D. thesis, Yale University
Koopmann, R. A. & Kenney, J. D. P. 1998, ApJ, 497, L75
Kornreich, D. A., Haynes, M. P., Lovelace, R. V. E., & van Zee, L. 2000, AJ, 120, 139
Larson, R. B., Tinsley, B. M., & Carswell, C. N. 1980, ApJ, 237, 692
Leonardi, A. J., & Rose, J. A. 1996, AJ, 111, 182
Lewis, I., *et al.* 2002, MNRAS, 334, 673
Lufkin, E. A., Sarazin, C. L., & White, III, R. E. 2000, ApJ, 542, 94
Magri, C., Haynes, M. P., Forman, W., Jones, C., & Giovanelli, R. 1988, ApJ, 333, 136
Melnick, J., & Sargent, W. L. W. 1977, ApJ, 215, 401
Mihos, J. C., McGaugh, S. S., & de Blok, W. J. G. 1997, ApJ, 477, L79
Moore, B., Katz, N., Lake, G., Dressler, A., & Oemler, A., Jr. 1996, Nature, 379, 613
Moore, B., Lake, G., & Katz, N. 1998, ApJ, 495, 139
Moore, B., Lake, G., Quinn, T., & Stadel, J. 1999, MNRAS, 304, 465
Mulchaey, J. S., Zabludoff, A. I. 1998, ApJ496, 73
Nichol, Robert C., Miller, C. J., & Goto, T. 2003, Ap&SS, 285, 157
Nilson, P. 1973, Uppsala General Catalogue of Galaxies (Uppsala: Astronomiska Observatorium) (UGC)
Nulson, P. E. J. 1982, MNRAS, 198, 1007
Oemler, A., Jr. 1974, ApJ, 194, 1
Ostriker, E. C., Huchra, J. P., Geller, M. J., & Kurtz, M. J. 1988, AJ, 96, 1775
Pfenniger, D. 1993, in IAU Symp. 153, Galactic Bulges, ed. H. De Jonghe & H. J. Habing (Dordrecht:Klewer), 387
Poggianti, B. M., & Barbaro, G. 1996 A&A, 314, 379
Poggianti, B. M., Smail, I., Dressler, A., Couch, W. J., Barger, A. J., Butcher, H. R.,; Ellis, R. S., & Oemler, A., Jr. 1999 ApJ, 518, 576
Richter, O.-G. & Sancisi, R. 1994, A&A, 290, L9
Rix, H.-W., & Zaritsky, D. 1995, ApJ, 447, 82
Rubin, V. C., Whitmore, B. C., & Ford, W. K. 1988, ApJ, 333, 522
Sakai, S., Giovanelli, R., & Wegner, G. 1994, AJ, 108, 33
Scodeggio, M., Solanes, J. M., Giovanelli, R., & Haynes, M. P. 1995, ApJ, 444, 41
Silverman, B. W. 1986, Density Estimation for Statistics and Data Analysis (London: Chapman & Hall)
Solanes, J., Manrique, A., García-Gómez, C., González-Casado, G., Giovanelli, R., & Haynes, M. P. 2001, ApJ, 548, 97
Solanes, J. M., & Salvador-Solé, E. 1992, ApJ, 395, 91
Solanes, J. M., Giovanelli, R., & Haynes, M. P. 1996, ApJ, 461, 609
Sperandio, M., Chincarini, G., Rampazzo, R., & de Souza, R. 1995, A&AS, 110, 279
Spitzer, L., Jr., & Baade, W. 1951, ApJ, 113, 413
Steinmetz, M. 1996 MNRAS, 278, 1005
Steinmetz, M. & Mueller, E. 1993 A&A, 268, 391
Struble, M. F., & Ftaclas, C. 1994, AJ, 108, 1
Sullivan, W. T., III, Bothun, G. D., Bates, B., & Schommer, R. A. 1981, AJ, 86, 919
Tarenghi, M., Chincarini, G., Rood, H. J., & Thompson, L. A. 1980, ApJ, 235, 724
Toomre, A., & Toomre, J. 1972, ApJ, 178, 623
van den Bergh, S. 1999, PASP, 103, 390
van Dokkum, P. G., Franx, M., Fabricant, D., Illingworth, G. D., & Kelson, D. D. 2000, ApJ, 541, 95
van Dokkum, P. G., Franx, M., Fabricant, D., Kelson, D. D., & Illingworth, G. D. 1999, ApJ, 520, L95
van Dokkum, P. G., Franx, M., Kelson, D. D., Illingworth, G. D., Fisher, D., & Fabricant, D. 1998, ApJ, 500, 714
Vikhlinin, A., Forman, W., & Jones, C. 1997, ApJ, 474, L7
Vogt, N. P. 1995, Ph.D. thesis, Cornell University
Vogt, N. P., Haynes, M. P., Herter, T., & Giovanelli, R. 2004a, ApJ, in press (Paper I)
Vogt, N. P., Haynes, M. P., Giovanelli, R., & Herter, T. 2004b, ApJ, in press (Paper III)
Vollmer, B. 2003, A&A, 398, 525
Vollmer, B., Braine, J., Balkowski, C., & Duschl, W. J. 2001a, A&A, 374, 824
Vollmer, B., & Huchtmeier, W. 2003, A&A, 406, 427
Vollmer, B., Cayatte, V., Balkowski, C., & Duschl, W. J. 2001b, ApJ, 561, 708
Vollmer, B., Cayatte, V., Boselli, A., Balkowski, C., & Duschl, W. J. 1999, A&A, 349, 411
Vollmer, B., Marcelin, M., Amram, P., Balkowski, C., Cayatte, V., & Garrido, O. 2000, A&A, 364, 532
Whitmore, B. C., Forbes, D. A., & Rubin, V. C. 1988, ApJ, 333, 542
Wu, X., Fang, L., & Xu, W. 1998 A&A, 338, 813
Zabludoff, A. I., Geller, M. J., Huchra, J. P., & Ramella, M. 1993a, AJ, 106, 1301
Zabludoff, A. I., Mulchaey, J. S. 1998, ApJ496, 39
Zabludoff, A. I., Zaritsky, D., Huan, L., Tucker, D., Hashimoto, Y., Schectman, S. A., Oemler, A., Jr., & Kirshner, R. P. 1996, ApJ, 466, 104
Zwicky, F., Herzog, E., & Wild, P. 1961 - 1968, Catalogue of Galaxies and of Clusters of Galaxies, I - VI (Pasadena: California Institute of Technology) (CGCG)